NARROW SPECTRAL WIDTH GENERATION BASED ON NONLINEAR MULTI-STEP MICRORING RESONATORS

PONGPUTHAI UDOMARIYASAP

A THESIS SUBMITTED IN PARTIAL FULFILLMENT
OF THE REQUIREMENT FOR THE DEGREE OF
DOCTOR OF ENGINEERING IN ELECTRICAL ENGINEERING
FACULTY OF ENGINEERING
KING MONGKUT'S INSTITUTE OF TECHNOLOGY LADKRABANG
2013

KMITL-2013-EN-D-018-015

หัวข้อวิทยานิพนธ์	การกำเนิดแสงที่มีความกว้างแถบที่แคบโดยใช้โพรงสั่นพ้องไม่เป็นเชิงเส้นขนาดเล็ก
นักศึกษา	นาย พงษ์ภูไท อุดมอริยทรัพย์
รหัสนักศึกษา	52610113
ปริญญา	วิศวกรรมศาสตรดุษฎีบัณฑิต
สาขาวิชา	วิศวกรรมไฟฟ้า
พ.ศ.	2556
อาจารย์ที่ปรึกษาวิทยานิพนธ์	ผศ. ดร. สุทธิชัย นพนาคีพงษ์

บทคัดย่อ

วิทยานิพนธ์นี้นำเสนอการสร้างสัญญาณความถี่สูงสำหรับใช้งานในระบบการสื่อสาร ซึ่งระบบการสร้างสัญญาณประกอบด้วยวงแหวนสั่นพ้องขนาดเล็กแบบไม่เป็นเชิงเส้นที่ต่ออนุกรมกันเป็นระบบที่สามารถใช้สร้างสัญญาณแบนด์วิดท์แบบพิเศษได้ สัญญาณอินพุทที่ป้อนให้กับระบบวงแหวนสั่นพ้องคือเกาส์เซียนพัลส์ที่กำหนดค่าความกว้างพัลส์ 200 nm ค่ากำลังแสง 2 W และศูนย์กลางความยาวคลื่นที่ 1500 nm โดยใช้กำหนดค่าความสัมพันธ์ของพารามิเตอร์ที่เหมาะสมกับอุปกรณ์ เช่น รัศมีของวงแหวน ค่าสัมประสิทธิ์การส่งผ่าน ค่าดรรชนีหักเหแบบเชิงเส้น เป็นต้น การเลือกสัญญาณออกมาใช้งานสามารถทำได้โดยใช้ตัวกรองทางแสงที่เรียกว่า "แอ็ดดร็อป (Add/Drop Filter)" ที่ควบคุมค่าพารามิเตอร์ของแอ็ดดร็อปทำให้ได้ค่ากำลังทางเอาต์พุตที่เหมาะสม นอกจากนี้เนื้อหาในวิทยานิพนธ์ยังนำเสนอผลงานที่น่าสนใจเกี่ยวกับการสร้างระบบมัลติพัลส์จากเกาส์เซียนพัลส์ที่ผลลัพธ์ภายหลังจากผ่านระบบวงแหวนสั่นพ้องแสดงให้เห็นถึงความเป็นไปได้ที่จะนำไปใช้สร้างระบบการกำเนิดสัญญาณหลายความยาวคลื่น (Multi Wavelength Generation) ในช่วงปลอดสเปคตรัม (Free Spectrum Range: FSR) ที่ 4.33 nm 2.15 nm 1.43 nm และ 1.05 nm และค่าความกว้างที่ครึ่งหนึ่งของกำลังสูงสุด (Full Width Half Maximum: FWHM) ที่ 0.132 nm, 0.067 nm, 0.046 nm and 0.033 nm ที่สามารถสร้าง และนำมาใช้ประโยชน์ในการขยายย่านความจุของช่องสัญญานในการสื่อสารทางแสงได้

Thesis Title	Narrow Spectral Width Generation Based on Nonlinear Multi-Step Microring Resonators
Student	Mr. Pongputhai Udomariyasap
Student ID	52610113
Degree	Doctor of Engineering
Program	Electrical Engineering
Year	2013
Thesis Advisor	Asst. Prof. Dr. Suthichai Noppanakeepong

ABSTRACT

This thesis, the generation of high frequency for communication system is proposed. The generation system consists of nonlinear microring resonator which integrated in a series scenario in order to produce the special bandwidth. The input signal is Gaussian pulse with 200 nm pulse width, 2 W peak power, and center wavelength at 1500 nm that propagate within microring resonator system. To generated the suitable output, the appropriate parameters relating to the practical device such as micro ring radii, coupling coefficients, linear and nonlinear refractive indexes is selected. The selection of proper output can be filter by optical filter called "Add/Drop filter" which control by the appropriate Add/Drop parameters. In additional, the interesting of multi pulse generator from Gaussian is presented. The results of microring resonator system indicate the possibility of Multi Wavelength Generation in Free Spectrum Range (FSR) range are 4.33 nm, 2.15 nm, 1.43 nm and 1.05 nm respectively and Full Width Half Maximum (FWHM) range are 0.132 nm, 0.067 nm, 0.046 nm and 0.033 nm. This system can be plausible and exploit for increasing the channel capacity in optical communication.

ACKNOWLEDGEMENTS

First of all, I would like to thank for the financial support of research project from Telecommunications Research and Industrial Development Institute (TRIDI), National Telecommunication Commission of Thailand (NTC), whose support made the completion of this work and my dream of graduate education come true

I would like to express my greatest appreciation and my gratitude to my advisor, Asst.Prof.Dr. Suthichai Noppanakeepong for his generous support and guidance.

I would like to thank Prof.Dr. Preecha Yupapin, for his profound insight into physics and stimulated assignments me not only to understand but also to solve and move fast forward through many challenging problems.

I would like to thank Associate Professor Dr. Somsak Mitatha , Dr. Nithiroth Pornsuwancharoen and Narongchai Moongfangklang for their assistance, helpful comments, and insightful suggestions.

I would also like to thank every young members of the Advanced Research Center of Photonic Laboratory (ARCP) of the Department of Applied Physics, Faculty of Science, King Mongkut's Institute of Technology Ladkrabang.

Finally, I would like to thank my loving parents who have taught me to achieve my goals, and my sister who have always believed in me. With their unconditional love, they has been the greatest supporters and a significant source of energy to me.

Pongputhai Udomariyasap

CONTENTS

CONTENTS (cont.)

LIST OF TABLES

Tables

LIST OF FIGURES

Figures

LIST OF FIGURES(cons.)

Figures

Pages

CHAPTER 1

INTRODUCTION

This chapter includes motivation of work, aim of work, structure of thesis and providing some fundamentals in subject of ring resonator. Ring resonators are presented in a relatively simple and straightforward way to give a tour through the subject by theoretical explanations.

1.1 Motivation

Ever since the explosive growth of communication technology, there has been an enormous demand for larger bandwidth in data transmission. Given the fact that a single-mode fiber is potential bandwidth nearly 50Tb/s, which is almost four orders of magnitude higher than electronic data rates of a few Gb/s. Optical communication systems is one of the most effective solutions to communicate the ever-growing need. Not only it is the potential to provide huge bandwidth, but it is also capable of providing low signal attenuation, low signal distortion, low power consumption, and greatly enhanced security [1]. This thesis investigates a relatively new highly attractive technology for optical communication such as microring resonators. Furthermore, one of the first papers dealing with the simulation of an integrated ring resonator for a bandpass filter has been published by Marcatili in 1969 [2, 3]. The basic configuration consists of unidirectional coupling between a ring resonator with radius r and a waveguide based on Yariv [4, 5]. There are different kinds of requirements on the simulation of various kinds of ring resonator configurations starting with the given equations satisfies most basic models. The ring model can be divided into more segments to account for different materials or modified waveguide paths. For examples of calculated models can be found in Rabus [6] and Michelotti et al. [7], and THz technology has become the interesting subject of investigation because it can be fulfilled the large demand of users in the future in terms of channel capacity. There are many researches which have been investigated in both theory and experiment [8-10] on THz technology involving in modern communication technology [11, 12]. Recently, Mitatha and his colleagues [13] shown the simultaneous short wave and millimeter wave generation. By using a soliton pulse within a nano-waveguide can be generated by a single small device and the simultaneous operation advantageously.

Moreover, the generated signals is stored within the system which is confirmed by Yupapin and Suwancharoen [14]. However, the problem of cut-off wavelength of light propagating within the proposed device has become a problem of the continuous research works in the areas of meta-materials [15]. Up to date, light pulse with wavelength up to sub millimeter wave can be confined within such a device [16]. In this work, the simulation of THz carrier frequencies using the small device and a Gaussian beam is feed to propagate within the device system is proposed. Consequently, the generated output power with the THz frequency can be achieved. Furthermore, the good FSR results have shown that they can be used to separate the adjacent outputs, and the spatial simulation output is also demonstrated showing the use of the very high output power within the small device is plausible. Microring resonators have also found various applications in photonics and optical communication systems [17]. From their excellent wavelength selectivity, compact size, and versatile functionalities have enabled them to be considered as potential building blocks in the future photonic integrated circuit (PIC) in near future.

1.2 Optical Ring Resonator

Nonlinear fiber optics has continuously to grown during the decade of 1990s, perhaps even more dramatically than anticipated. This growth is motivated by several recent advances in lightwave technology, the most important being the advent of high-capacity fiber-optic communication systems. A variety of nonlinear optical signal processing functions in microring resonator can be realized in many applications; for examples, the Kerr effect, four wave mixing (FWM) can be used for communication at high microwave frequency (THz); the Add/Drop multiplexing can be used for cancellation chaotic signal, and the chaos of nonlinear system can be chaos communication application.

The theoretical background of ring resonator starts with general considerations of ring resonator and the used model for single coupler ring resonator filter and double coupler ring resonator filter. Presenting a very fascinating simulation of light pulses traveling within a ring resonator system that has revealed unexpected results for various applications, especially in optical communication. The design system consists of a nonlinear microring resonator system incorporating with Add/Drop filter. Input light pulse is Gaussian pulse, whereas the suitable simulation parameters are input power, pulse width, ring radii, and the material refractive indices.

1.2.1 Ring Resonator

A ring resonator is simply a waveguide shaped into a ring structure as shown in figure 1.1. Whenever an input electric field, E_i, is coupled to the ring waveguide through an external bus waveguide, a positive feedback is induced and the field inside the ring resonator E_r, starts to build up. Coupling between the straight and the ring waveguide is achieved through the evanescent wave. Therefore, the gap and coupling length between them determine how much power is coupled from the straight waveguide to the ring waveguide and vise versa. The feedback mechanism is simply induced by the ring waveguide; furthermore, there is no need for any Bragg Gratings, mirrors, or distributed feedback waveguides which are more difficult to fabricate. In such configuration, only certain wavelengths will be allowed to resonate inside the ring waveguide, thus frequency selectivity is obtained. A resonant mode have a wavelength that satisfies [18].

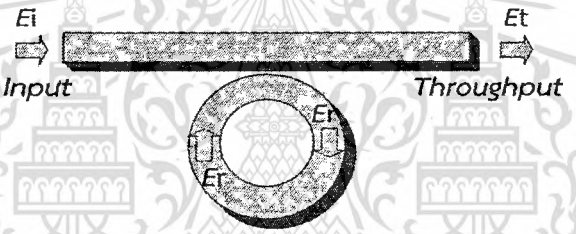

Figure. 1.1 Schematic diagram for a ring resonator coupled to a single waveguide.

$$m\lambda_m = nL, \quad \text{m = integer} \tag{1.1}$$

where m is the longitudinal mode number.

λ_m is the resonant mode wavelength.

n is the refractive index of the guiding material.

L is the circumference of the ring resonator.

The electric field circulating inside the resonator is given by [19].

$$E_r(t) = -j\kappa E_i(t) + rae^{j\phi}E_r(t-\tau) \tag{1.2}$$

where κ and r are the field coupling and transmission coefficients between the straight and ring waveguides such that $\kappa^2 + r^2 = 1$, τ is the round trip time of the ring resonator.

The round trip field transmission, a is given by

$$a = e^{-\alpha_o L/2} \tag{1.3}$$

where α_0 is the propagation loss inside the microring in mm^{-1}.

The resonator round trip phase, ϕ is given by

$$\phi = \frac{2\pi}{\lambda} nL \tag{1.4}$$

The transmitted or throughput field at the output of the straight waveguide, E_t is given by

$$E_t(t) = rE_i(t) - j\kappa a e^{j\phi} E_r(t-\tau) \tag{1.5}$$

At steady state, the transmission-transfer function of the resonator can be written as

$$\frac{E_t}{E_i} = \frac{r - ae^{j\phi}}{1 - rae^{j\phi}} \tag{1.6}$$

1.2.2 Optical Add/Drop Filter

Add/Drop filter is similar to a Fabry-Perot interferometer, the ring geometry permits more than one waveguide to be coupled to the ring resonator [11]. On the other hand, it allows multiple input/output accessibility without external circulators to manipulate the input and reflect throughput data streams. For instance, if one more waveguide is coupled to the phase filter described earlier, an optical add/drop filter is obtained, as shown in figure 1.2. At steady state, the transmission-transfer function at the drop and throughput ports are given by

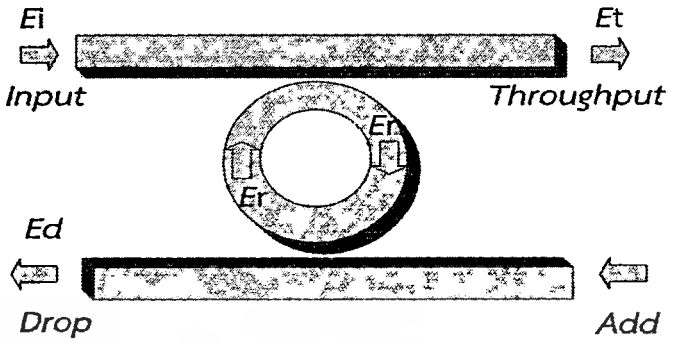

Figure 1.2 Schematic diagram for a ring resonator coupled to two waveguides, in an Add/drop filter configuration.

Drop port:

$$\frac{E_d}{E_i} = \frac{-\kappa_1 \kappa_2 a^{1/2} e^{j\phi/2}}{1 - a r_1 r_2 e^{j\phi}} \tag{1.7}$$

Throughput port:

$$\frac{E_t}{E_i} = \frac{r_1 - a r_2 e^{j\phi}}{1 - a r_1 r_2 e^{j\phi}} \tag{1.8}$$

where κ_1 and r_1 are the field coupling and transmission coefficients between the ring and the input waveguide while κ_2 and r_2 are the field coupling and transmission coefficients at the output waveguide. An interesting criterion of this device can be observed in above equation. A complete power transfers between the input port and the drop port is obtained at resonance $\phi = 0$, for a lossless microring resonator that has a symmetric coupling, i.e. $\kappa_1 = \kappa_2$. At the same time, the throughput port will have a complete extinction, thus this condition is referred to as critical coupling in analogy with what have been discussed earlier in subsection microring resonator.

1.3 Goal of the Thesis

Currently, a numerous demand of larger bandwidth for data transmission is a once factor to drive the effective of optical communication. In order to response the communication demand, this thesis will concentrate in three goals, there are :

1. Design the microring resonator system which generate the high frequency for communication system.
2. Confirmation the generated Multi Wavelength Generation that utilized for optical network communication.
3. Confirmation the generated high frequency of microring resonator system by results of FSR and FWHM.

1.4 Scope of the Thesis

Design microring resonator system from transfer function and assign parameters of nonlinear microring resonator (GaInAsP/InP) for generated high frequency signal for communication system. Normally, nonlinear behavior in a ring resonator consist of the Kerr effect as chaotic phenomenal, which appears to the penalty and benefits the communication systems. Accompany with the design parameters from transfer function of microring resonator (Add/Drop filter) for filter output signal from nonlinear microring resonator for optical communication application is confirm. Finally, we show that the control input power and ring parameter such as a coupling coefficient, ring radii for generated signal can be used to specify the output filtering signal which can be simulated by Matlab program.

1.5 Outline of the Thesis

This thesis presents simulation and design of microring resonator and application. The outline is as follow:

Chapter 1 Introduction.
Chapter 2 Theoretical Background.
Chapter 3 Calculation Models of Ring Resonators
Chapter 4 Narrow Spectral Width Generation Based on Nonlinear Multi-Step Microring Resonators
Chapter 5 Conclusion and Future Work.

CHAPTER 2

THEORETICAL BACKGROUND

This chapter present the theoretical background for a good understanding the multi wavelength and high frequency generation of proposed system which mentioned in chapter 4. The organization of chapter compose of optical filter, characterization of ring resonator, Fabry-Perot interferometer and nonlinear fiber optic.

2.1 Optic Filter

Since, our system using optical filter fitter for output of communication system, therefore the notion of optical filter is needed. Normally, the optical filter is categorized into 2 classes as follow:

2.1.1) Finite impulse response (FIR) or moving average (MA) filters is filter do not rely on any feedback mechanism, i.e., optical reflections. These filters are sometimes called "feed forward". For the instant of Mach-Zehnder based filters and waveguide grating routers (WGRs).

2.1.2) Infinite impulse response (IIR) or autoregressive (AR) filters is filter inherently are based on multiple reflections. Examples of these class include fiber bragg gratings (FBGs), thin film filter (TFFs), and optical all-pass filters (APFs).

The description of some of the most common optical filters [21] is given by:

a) Plane Grating

A typical reflective grating consists of a mirrored surface with tiny periodically located grooves. When it illuminates the light reflected from one groove interfering with the reflected light from other grooves resulting in constructive and destructive interferences. The wavelength dependence of the interference patterns is exploited to separate the different wavelengths which are detected for examples by using a photodiode.

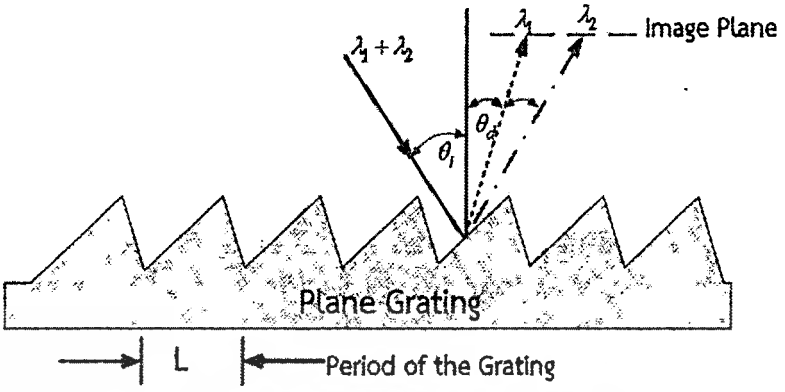

Figure 2.1 Plane grating.

b) Fabry-Perot Interferometer

The principle of this filter was invented in 1898 by the French physicists, Charles Fabry and Alfred Perot, which occur between two highly reflective parallel mirrors are separated by a small distance. Most of the light that encounters the first mirror is reflected, but some of it transmits, travel through the cavity (the space between the mirrors is often filled with some kind of dielectric e.g. liquid crystals (LCs)), and strike the second mirror. At the second mirror, most of the light is reflected, while some transmit. The reflected light travels backwards hitting the first mirror, where some of it again reflect and some transmit. The result depends on space and index of refraction between the mirrors, and at some wavelengths the multiple reflections interfere constructively. At these wavelengths, the cavity resonates, some of the light passes through. As for other wavelengths, the transmitted waves add out of phase and the reflected waves add in phase. Moreover, the interferometer overall transmission is low, and the overall reflectivity is high.

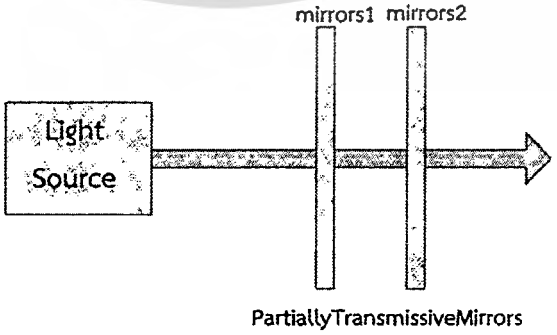

Figure 2.2 Fabry Perot interferometer.

c) Fiber Bragg Grating [22].

These types of filters consist of a region in which the index of the fiber varies periodically between high and low, and they are formed in optical fibers by exposing the fiber to interferometric patterns from an ultraviolet (UV) laser. As in the Fabry-Perot interferometer, multiple reflected and transmitted waves are the result. For a specific wavelength, the reflected waves all add in phase, and wavelength the grating appears to be highly reflective, while transmits all the others.

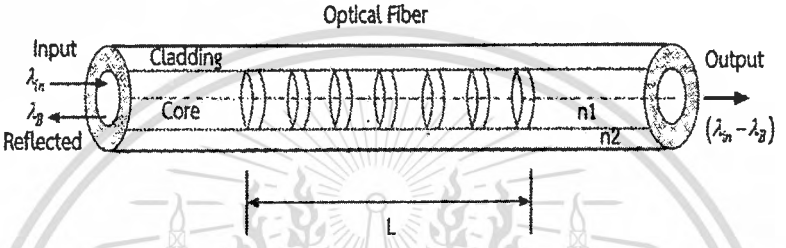

Figure 2.3 Optical fiber Bragg grating.

d) Arrayed Waveguide Grating (AWG) [23]

The most common filter in optical telecommunications is AWG of filter. The AWG uses an array of single mode waveguides in which the lengths of adjacent waveguides differ by fixed amount. The input light from a single fiber illuminates all these waveguides. Because of the different lengths of the waveguides, the phase of the light (at the output end of the array of waveguides) varies by fixed amount from one waveguide to the next. This variation results in a wavelength dependent phase front that is similar to the one from a plane grating. This pattern is then arranged so that different wavelengths illuminate different output fibers. The AWG can serve as a wavelength multiplexer as well as a demultiplexer.

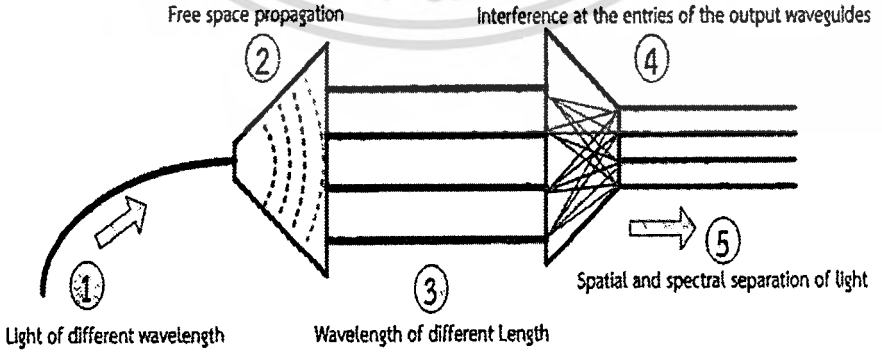

Figure 2.4 Arrayed Waveguide grating.

e) Mach-Zehnder Interferometer (MZI)

This filter consists of a pair of couplers connected by two paths of unequal length. Group velocity dispersion in the optical paths of different lengths results in some wavelengths being output to the top port and others being output to the bottom port.

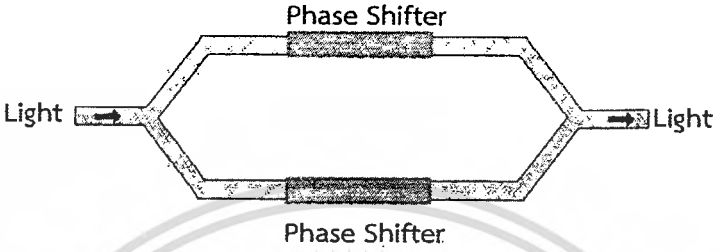

Figure 2.5 Mach Zehnder interferometer.

f) Thin Film Dielectric Interference Filter

This filter requires the deposition of many layers of coating to create narrow-band filters. A typical filter with a 3 dB bandwidth of 100 GHz requires more than a hundred layers of coating. With so many layers being deposited, errors are caused by local film thickness variation and alternation in increased density, reducing the yield of useful filters. A transmitted beam that goes through a filter is composed of multiple sub-beams; each has a slightly different travel time which adds dispersion to the data signal with a thin film metal interference filter and an all dielectric interference filter.

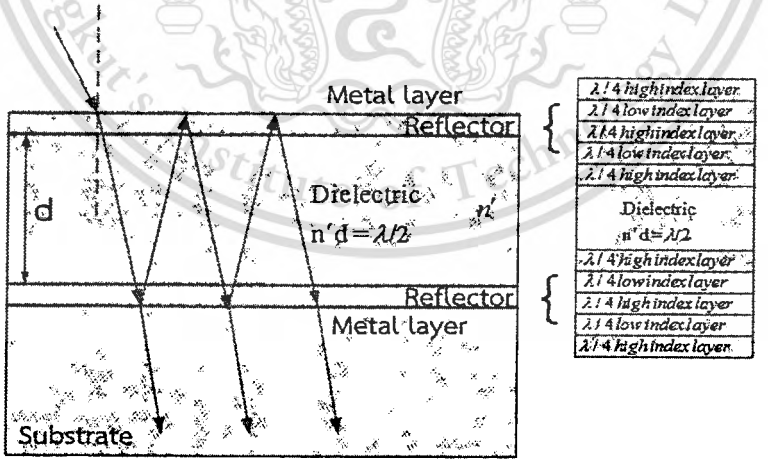

Figure 2.6 Thin film dielectric interference filter.

2.2 Characteristics of Ring Resonator and Fabry-Perot Interferometer

The most basic configuration of the microring resonator show in figures. 2.7 and 2.8 which consist of a ring-shaped waveguide coupled with either one or two optical waveguides. The cavity mode is excited by evanescent closely coupling to spaced optical waveguides, which function as semi-reflecting mirrors. Direct analogy can be drawn between recalculating and standing wave resonators. In the case of a ring resonator is coupled with one waveguide, one relates to a Gires-Tournois interferometer [24] partially and another totally reflecting mirror. Furthermore, if In the case of a ring resonator is coupled with two bus waveguides, one has a Fabry-Perot interferometer with partially two reflecting mirrors. Gires-Tournois interferometer is as similar as a Fabry-Perot interferometer, which has a resonated cavity consisting of two parallel reflective plates. However, one plate is fully reflective, whereas the other one is partly reflective. Hence, the Gires-Tournois Interferometer can only work in the reflective mode not in the transmission mode. The resonance condition is the same as with the Fabry-Perot.

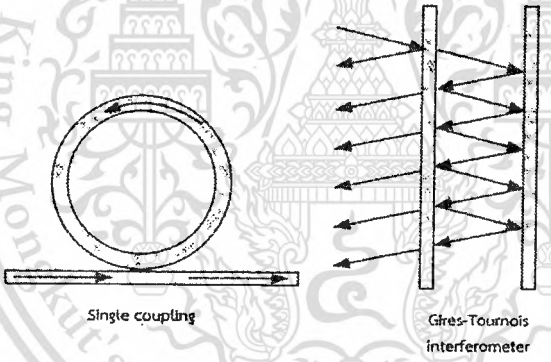

Figure 2.7 The schematics of traveling wave resonators and their standing wave analogs, Gires-Tournois Interferometer.

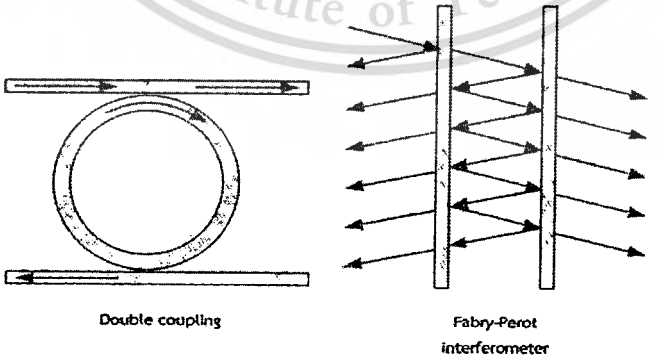

Figure 2.8 The schematics of traveling wave resonators and their standing wave analogs, Fabry-Perot interferometer.

2.3. Fabry-Perot Interferometer

A Fabry-Perot interferometer filter [25, 26] uses a multiple beam interference process for obtaining wavelength selectivity. Usually, the filter has one input and one output port and employs two highly reflecting plates which together constitute the resonating cavity creating the multiple beam interference process. The basic concept of an Fabry-Perot filter is shown in figure 2.9. It was described first by Charles Fabry and Albert Perot in 1898. Two highly reflective planar plates are accurately positioned in parallel and thus formed a cavity. A light beam entering the cavity is reflected multiple times between the plates, and each time the beam hits a plate; a small part of its power escapes. When the two plates are aligned perfectly in parallel, the multiple beam has a fixed phase difference respectively with the preceding one; this difference phase corresponds to the extra path length traveled in the cavity.

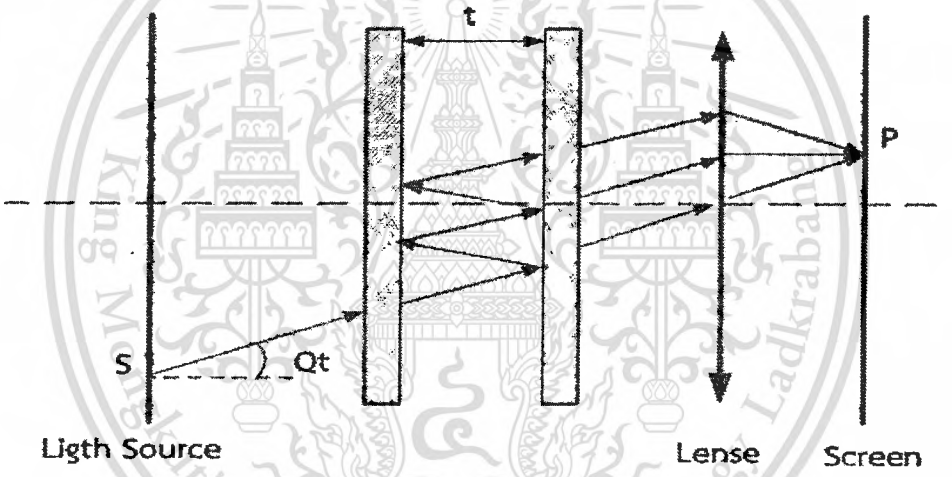

Figure 2.9 A schematic of Fabry-Perot interferometer.

The multiple parallel beams are brought into a common focus point with lens, and at this point the actual multiple beam interference takes place. Hence, the amplitude of the transmitted electrical field E_t can be described by the interference of multiple light beam in a Fabry-Perot interferometer, which contents of the two beams separated from the same source. The beam is reflected several times to get together with several aircrafts. Before studying the details of this kind, we should understand that the phenomena associated with the first beam is normally incident on the surface of the medium to any other pairs is the refraction through the intermediary of one and reflected back in the middle of it.

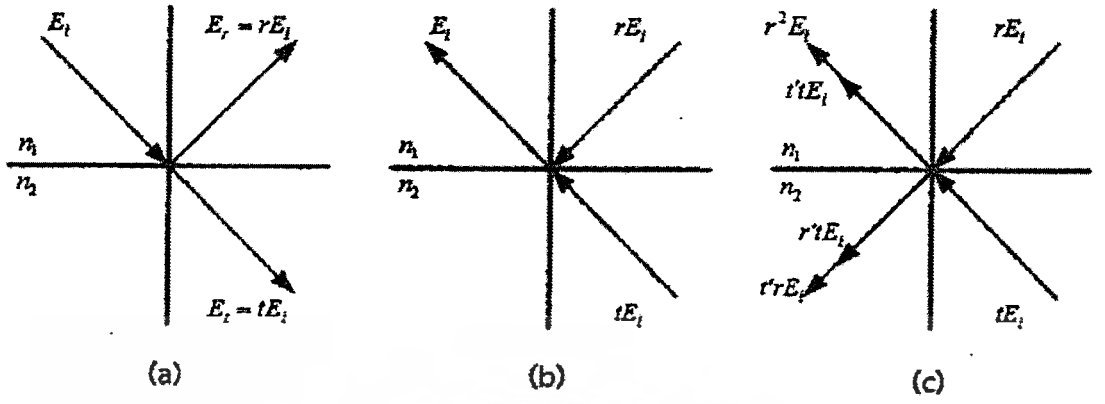

Figure 2.10. The reflection of light between the medium n_1 and n_2.

where E_i is the size of the incident light, E_r is the size of the reflector, and E_t stands for the size of the light through define them as followed.

The reflection coefficient:

$$r = \frac{E_r}{E_i} \tag{2.1}$$

The transmission coefficient:

$$t = \frac{E_t}{E_i} \tag{2.2}$$

Figure 2.10 (a) show a light ray or incident ray (E_i) propagate to material which is compost of two reflective index n_1 and n_2, then the light ray can be split into reflected ray (rE_i) and transmitted ray (tE_i). On the other hand, figure 2.10 (b) illustrate the reverse result of figure 2.10 (a) that the incident ray (E_i) is a summation of reflected ray (rE_i) and transmitted ray (tE_i) at a suture of material. For figure 2.10 (c) demonstrate reflected ray (rE_i) and transmitted ray (tE_i) at the suture of material in 2.10 (b) are reflect and refract, the rE_i ray will split into reflected ray $r(rE_i)$ and transmitted ray $t(rE_i)$, similarly, the tE_i ray will split into reflected ray $r'(tE_i)$ and transmitted ray $t'(tE_i)$. Here, it can be used to represent the reflection r' and refraction t' in an old pair moving from Medium n_2.

However, the situation is shown in figures. 2.10 (b) and 2.10 (c) given by

$$E_i = \left(r^2 + t't\right)E_i \tag{2.3}$$

and

$$0 = \left(r't + tr\right)E_i \tag{2.4}$$

Therefore

$$tt' = 1 - r^2 \tag{2.5}$$

$$r = -r^2 \tag{2.6}$$

The phase difference in π radians, which is external to the internal reflection will bring the above to be used in the study reflecting several times. Between the surface parallel in figure 2.11, the incident beams E_0 at an angle θ_i and the reflection r and transmission coefficient t in the external parts with a coefficient of reflection r' and transmission t' in the internal reflection. From this point can see that if the incident beam, only one beam is reflected back to the beam. When the beam is passed to the other side, it is reflected or refracted the beam of light in the interference between these species and can see by the light of the convex lens as shown in figure 2.11 in the case of light refracted through The phase difference (δ) of reflected light is given by:

$$\delta = k\Delta \tag{2.7}$$

When $\Delta = 2n_f t\cos\theta_t$ with using the refractive index n_f and the thickness film t parallel to the surface respectively, it can write in the form of light $E_0 e^{i\omega t}$ and a light reflecting surface of the film as follows:

$$
\begin{aligned}
E_1 &= \left(rE_0\right)e^{i\omega t} \\
E_2 &= \left(tt'r'E_0\right)e^{i(\omega t-\delta)} \\
E_3 &= \left(tt'r'^3E_0\right)e^{i(\omega t-2\delta)} \\
E_4 &= \left(tt'r'^5E_0\right)e^{i(\omega t-3\delta)} \\
&\vdots \\
E_N &= \left(tt'r'^{(2N-3)}E_0\right)e^{i(\omega t-(N-1)\delta)}
\end{aligned}
\tag{2.8}
$$

when these waves are the same as well E_R.

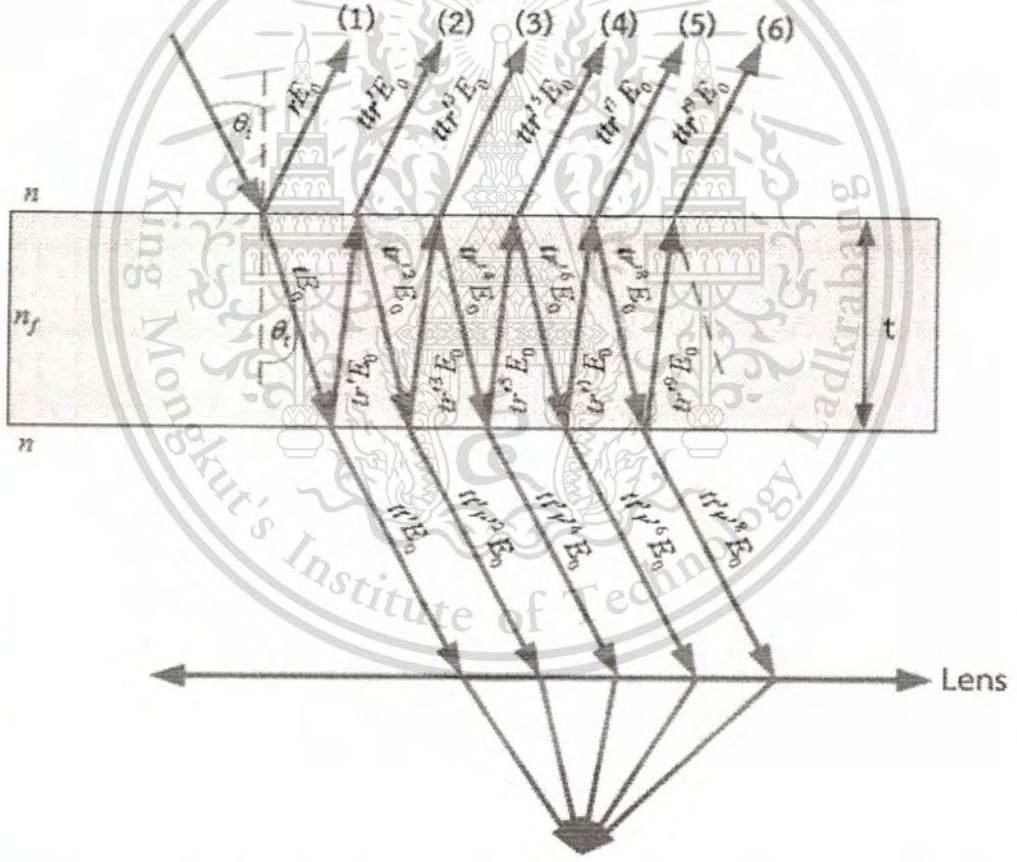

Figure 2.11 The reflection and refraction of the medium in parallel with the surface.

$$E_R = \sum_{N=1}^{\infty} E_N = rE_0 e^{i\omega t} + \sum_{N=2}^{\infty} tt' E_0 r'^{(2N-3)} e^{i[\omega t-(N-1)\delta]}$$

$$E_R = E_0 e^{i\omega} t\left[r + tt' r' e^{i\delta} \sum_{N=2}^{\infty} r'^{(2N-4)} e^{-i(N-2)\delta} \right] \tag{2.9}$$

The summation of equation above is takes in the form of $\sum_{N=2}^{\infty} x^{N-2} = 1 + x + x^2 + \ldots$

Since these series converge $|x| < 1$ as that summation is $\frac{1}{1-x}$

$$E_R = E_0 e^{i\omega t}\left(r + \frac{tt' r' e^{-i\delta}}{1 - r'^2 e^{-i\delta}} \right) \tag{2.10}$$

The correlation function of equations. (2.5) and (2.6) given by

$$E_R = E_0 e^{i\omega t}\left[r - \frac{\left(1 - r^2\right) r e^{-i\delta}}{1 - r^2 e^{-i\delta}} \right] \tag{2.11}$$

The light intensity I is the product of E_R and the conjugate E_R^*.

$$\left|E_R\right|^2 = E_R E_R^* = E_0^2 r^2 \left[\frac{e^{i\omega t}\left(1 - e^{-i\delta}\right)}{1 - r^2 e^{-i\delta}} \right]\left[\frac{e^{i\omega t}\left(1 - e^{-i\delta}\right)}{1 - r^2 e^{-i\delta}} \right] = E_0^2 r^2 \left[\frac{2 - e^{i\delta} - e^{-i\delta}}{1 + r^4 - r^2\left(e^{i\delta} - e^{-i\delta}\right)} \right] \tag{2.12}$$

For simplify equation, substitute (2.13) into equation (2.14).

$$\frac{e^{i\delta} + e^{-i\delta}}{2} \approx \cos\delta \tag{2.13}$$

$$\left|E_R\right|^2 = E_0^2 r^2 \left[\frac{1 - \cos\delta}{1 + r^4 - 2r^2 \cos\delta} \right] \tag{2.14}$$

In order to determine light intensity I_R, so that the production of incident light intensity I_i is essential as shown in equation (2.15).

$$\frac{I_R}{I_i} = \frac{\left|E_R\right|^2}{\left|E_0\right|^2} \tag{2.15}$$

From equation (2.16), I_R is the reflection Intensity as show in the following equation

$$I_R = \left[\frac{2r^2(1-\cos\delta)}{1+r^4-2r^2\cos\delta} \right] I_i \qquad (2.16)$$

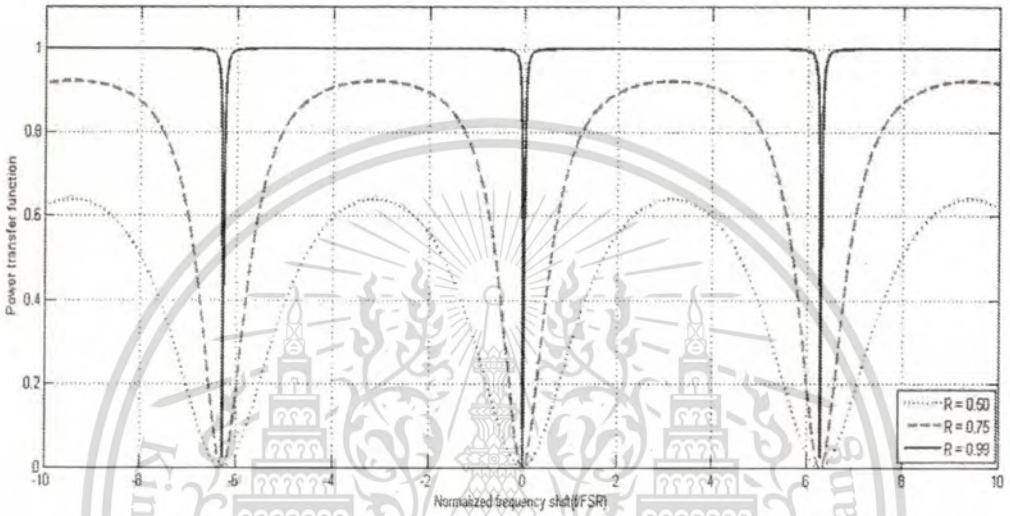

Figure 2.12 The Reflected of the Fabry-Perot interferometer.

One of important factor in the design of the filter is the contrast factor which is defined primarily as the ratio of the maximum to minimum reflection, and the ratio in the intensity reflection values of the peaks and the troughs shown in figure 2.12. In the same way, will find that for a beam of light is transmitted to the other side, and the light intensity equation of Fabry-Perot Interferometer is very similar to a ring resonator, shown in chapter 1.

From equation (2.16), I_T is the transmission Intensity as demonstrate below

$$I_T = \left[\frac{(1-r^2)^2}{1+r^4-2r^2\cos\delta} \right] I_i \qquad (2.18)$$

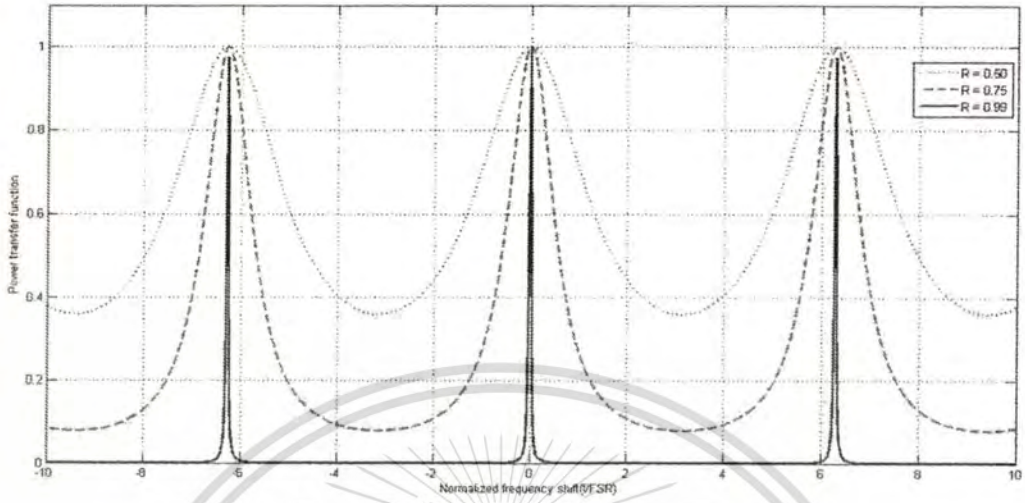

Figure 2.13 The Transmitted of the Fabry-Perot interferometer.

Another important factor in the design of the filter is the contrast factor which is defined primarily as the ratio of the maximum to minimum transmission, and the ratio in the intensity transmission values the peaks and the troughs shown in figure 2.13. However, the field propagating inside the ring cavity is a traveling wave in contrast to the Fabry-Perot cavity which resonates a standing wave.

2.4 Nonlinear Fiber Optics

Nonlinear optic is the branch of optics that describes behavior of light in nonlinear media which the dielectric polarization responds nonlinearly to the electric field of the light. This nonlinearity is typically only observed at very high light intensities such as those provided by pulsed lasers.

Glass fibers for optical communications are made of fused silica, an amorphous material, which dopant materials of various kinds can be added to produce changes in refractive index. A number of third order nonlinear processes can occur, and these can grow to appreciable magnitudes over the long lengths available in fibers. Even though the nonlinear coefficients in the materials are relatively small, the effects are particularly important in single-mode fibers which the small mode field dimensions result in substantially high light intensities with relatively modest input powers.

Fiber nonlinearities fall into two general categories [27]. The first category of nonlinearities arises from modulation of the refractive index of silica by intensity changes in the signal (Kerr effect). This gives the rising to nonlinearities such as self-phase modulation (SPM), whereby an optical signal alters its own phase; cross-phase modulation (CPM or XPM). Where one signal affects the phases of all others optical signals and vice-versa and four-wave mixing (FWM), signals with different frequencies will interact to produce mixing sidebands. The second category of nonlinearities corresponds to stimulated scattering processes, such as Stimulated Brillouin Scattering (SBS) and Stimulated Raman Scattering (SRS) which are interactions between optical signals and acoustic or molecular vibrations in the fiber. These effects become important in long optical links operated at high optical power levels. In single-wavelength systems, SPM, SRS, and SBS is a cause of pulse distortion and attenuation. In addition, in DWDM systems, CPM, SRS, SBS, and FWM can also cause crosstalk between optical channels.

Fiber nonlinearities have different influences on the communication systems. The SPM, for instance, leads to a change in the dispersion behavior in high-bit-rate transmission systems; the XPM, SRS, and SBS determine a decrease of the signal to noise ratio; the SRS and FWM will increase the crosstalk between different WDM channels. On the other hand, the same nonlinear effects offer a variety of possibilities for ultrafast all-optical switching, amplification, and regeneration [28].For example the FWM, SRS, and SBS are able to amplify optical signals in spectral ranges that never reached by erbium-doped fiber amplifiers. Moreover, the FWM offers the possibility for a pure optical wavelength conversion and the realization of nonlinear optical phase conjugation which compensate completely the distortions of the optical pulses. Optical solitons offer the possibility of transmitting optical pulses over extremely large distances without distortion [29, 30].

2.4.1 Self Phase Modulation

The change in refractive index due to the Kerr effect determines from a corresponding change in the propagation constant. As a consequence, the phase of a signal propagating through the fiber varies with distance according to the equation;

$$\phi = n_0 k_0 z + \gamma P(t) z \tag{2.19}$$

According to $\gamma = n_2 k_0 / A_{eff}$ the first term in equation (2.19) represents the linear phase shift due to signal propagation, and the second term represents the nonlinear phase shift. Also, when the incident wave is a pulse with a power variation given by *P*(*t*), the output pulse is chirped. This phenomenon is called self-phase modulation (SPM), since the power variation within the pulse leads to its own phase modulation. In the leading edge of the pulse, where $dP/dt > 0$ the instantaneous frequency is downshifted from the central frequency, whereas in the trailing edge where $dP/dt < 0$ the instantaneous frequency is upshifted. The chirping due to nonlinearity leads to increased spectral broadening.

In the presence of dispersion, the spectral broadening due to SPM determines two situations qualitatively different. In the normal dispersion region (where the wavelength is shorter than the zero dispersion wavelength, λ_{ZD}), the chirping from dispersion downshifts the leading edge and upshifts the trailing edge of the pulse, which is a similar effect as SPM. Thus, in this regime the chirping due to dispersion and SPM add. On the other hand, in the anomalous dispersion region, the chirping because of dispersion is opposite to SPM. Consequently, nonlinearity and dispersion induced chirpings can partially or even completely cancel each other. When this cancellation is total, the pulse neither broadens in time nor in its spectrum and such pulse is called a soliton. Much research effort has been devoted to the study of optical solitons and their application in telecommunication systems because they have the peculiar behavior of preserving their shape during propagation [31]

2.4.2 Cross Phase Modulation

When two or more signals having different carrier frequencies are transmitted simultaneously inside an optical fiber, the nonlinear phase evolution of the signal at frequency ω_i depends on the power of the other signals. This nonlinear phenomenon is known as a "cross phase modulation (XPM)" and which occur from the intensity dependence of the refractive index. The nonlinear phase shift of the signal at ω_i becomes:

$$\phi_i^{NL} = \gamma z \left[P_i + 2 \sum_{i \neq j} P_j \right] \tag{2.20}$$

Where P_j is the power of the signal at ω_j, the first term in the square brackets represents the contribution of SPM, while the second term is the contribution from the XPM. The factor 2 in equation (2.20) indicates that XPM is twice as effective as SPM for the same amount of power. From equation (2.20) is deduced which imply that XPM is effective only when the interactive signals are superimposed in time. In the presence of finite dispersion, two pulses at different frequencies will move with different velocities, and thus the pulses will walk off from each other. Obviously, larger dispersion will reduce the walk off length and the XPM effects.

Due to XPM, the phase of each channel in a WDM system is affected by both the average power and the bit pattern of all other channels. Fiber dispersion converts phase variations into amplitude fluctuations that affect the signal-to-noise ratio (SNR) and introduce jitter. In these circumstances, an understanding of the interplay between XPM and GVD is very important for WDM systems [32].

2.4.3 Four Wave Mixing

When the signal at difference frequencies propagates through the medium besides XPM, another important effect called "four wave mixing (FWM)" is occurred [27]. Four wave mixing is a nonlinear effect arising from a third-order optical nonlinearity, as is described with a $\chi^{(3)}$ coefficient. It can be occurred if at least two different frequency components propagate together in a nonlinear medium such as an optical fiber assuming just two input frequency components ω_1 and ω_2 (with $\omega_2 > \omega_1$). Then a refractive index modulation at the difference frequency occurs and creates additional frequency components. As a result, two new frequency components are generated: $\omega_3 = \omega_1 - (\omega_2 - \omega_1) = 2\omega_1 - \omega_2$ and $\omega_4 = \omega_2 + (\omega_2 - \omega_1) = 2\omega_2 - \omega_1$ shown in figure 2.14.

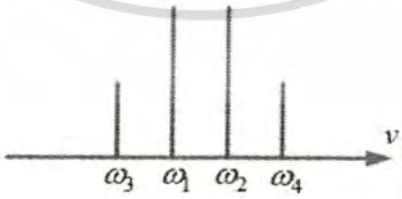

Figure. 2.14 Generation of new frequency components by four wave mixing.

Four wave mixing (FWM) is a parametric interaction among waves satisfying a given phase relationship called "phase matching". Different phenomena may be originated by FWM process depending on the relation among interaction frequencies. If three optical fields with carrier frequencies ω_i (i = 1, 2, 3) co-propagate inside the medium simultaneously, it appears that the third-order polarization vector has several components, three components have the frequencies of the input fields, and the others have an angular frequency ω_4 given by

$$\omega_4 = \omega_1 \pm \omega_2 \pm \omega_3 \tag{2.21}$$

If no field is presented in the medium at the frequency ω_4, a new field component is created at this frequency. In addition, if a field at the frequency ω_4 is already presented in the medium, it will be affected by the nonlinear interaction between the fields at ω_i, which causes crosstalk in multi-channel communication systems.

The phase-mismatch among all for waves is given by

$$\Delta\beta = \beta(\omega_1) + \beta(\omega_2) - \beta(\omega_3) - \beta(\omega_4) \tag{2.22}$$

where $\beta(\omega)$ is the propagation constant for an optical field with frequency ω, can assume the frequencies closely and equally spaced (i.e., $\omega_1 = \omega_2 - \Delta\omega$, $\omega_3 = \omega_2 - 2\Delta\omega$, $\omega_1 = \omega_2 - \Delta\omega$) and making a Taylor series expansion of all β is about the frequency ω_2, therefore:

$$\Delta\beta = 2\beta_2(\Delta\omega)^2 \tag{2.23}$$

where $\beta_2 = \partial^2\beta / \partial\omega^2$ is the group velocity dispersion (GVD), and $\beta_2 = 0$ a perfect shave-phase matches an efficient FWM. This situation is desirable for applications such as all-optical signal processing, wavelength conversion, pulse compression, etc. FWM in optical materials can also be used for generating spectrally inverted signal through the process of optical phase conjugation (OPC), which is useful for dispersion compensation. However, in WDM systems FWM causes a transfer of power from each channel to its neighbors. Such a power transfer is not only resulted in the power loss for the channel but also induces inters channel crosstalk that degrades the system performance severely. This problem can be minimized using the technique of dispersion management, in which the dispersion is kept locally high even though it is low on average.

CHAPTER 3

CALCULATION MODELS OF RING RESONATORS

This chapter will describe the material system which is used for the planar waveguide such as the theoretical of ring resonator, nonlinear characteristics of ring resonators, fiber optic ring resonators, and the processes that affect the performance of semiconductor microring resonator system that used for optical signal processing tools.

The use of semiconductor materials as nonlinear optical elements bridges the gap between optics and electronics. It opens the possibility for integrating the laser sources, signal processing elements, and detectors on the same platform. In this regard, the III-V binary semiconductors, such as GaAs and InP, have acquired great attention in the last few decades because they are direct band gap materials and possess higher nonlinear coefficients than their competing materials. Another attractive feature of binary semiconductors is that they can be combined or alloyed to form ternary or quaternary compounds. By doing so, makes it possibly to vary the band gap of the material continuously together with its band structure, electronic, and optical properties. As an example, the band gap energy of the ternary compound $Al_xGa_{1-x}As$ depends on the mole fraction x. This thesis will consider $In_{0.8}Ga_{0.2}As_{0.45}P_{0.55}$ which the refractive index (n_1) is 3.327 and $In_{0.8}P_{0.55}$; the refractive index (n_2) is 3.168. Therefore, one can design ternary and quaternary compounds to be transparent for optical channel waveguides or active for lasers and can amplifier at the 1550 nm communication window [42].

For an understanding of the nonlinear optics in waveguide, it is necessary to consider the theory of electromagnetic wave propagation in dispersive nonlinear media. The objective of this chapter is to discuss fiber characteristics, fiber nonlinearities and basic equation that governs propagation of optical pulses in single mode fibers. Furthermore the discuss nonlinear in optical fiber ring resonator such as Kerr effect , optical chaotic communication, and optical Add/Drop filter is presented.

3.1 Nonlinear Susceptibility

Nonlinear optics is the study of phenomena that occurs as a consequence of the modification of the optical properties of a material under intense illumination. Typically, only laser light is sufficiently intense to modify the optical properties of a material. Nonlinear optical phenomena is nonlinear in the sense that the induced material polarization is nonlinear in the electric field. The general equation that describes the optical field evolution in a dielectric material [43], considers form of the wave equation for the propagation of light through a nonlinear optical medium. Maxwell's equations write in gaussian units in the form using a tilde (~) in order to denote a quantity that varies rapidly in time.

$$\nabla \cdot \tilde{D} = 4\pi\tilde{\rho} \tag{3.1}$$

$$\nabla \cdot \tilde{B} = 0 \tag{3.2}$$

$$\nabla \times \tilde{E} = -\frac{1}{c}\frac{\partial \tilde{B}}{\partial t} \tag{3.3}$$

$$\nabla \times \tilde{H} = \frac{1}{c}\frac{\partial \tilde{D}}{\partial t} + \frac{4\pi}{c}\tilde{J} \tag{3.4}$$

The primarily interested in the solution of these equation in regions of space contains no free charges.

$$\tilde{\rho} = 0 \tag{3.5}$$

The contain of no free current,

$$\tilde{J} = 0 \tag{3.6}$$

and assuming the material is nonmagnetic.

$$\tilde{B} = \tilde{H} \tag{3.7}$$

However, the material is nonlinear in the sense that the fields $\tilde{D}$ and $\tilde{E}$ are related by

$$\tilde{D} = \tilde{E} + 4\pi\tilde{P} \tag{3.8}$$

Generally, the polarization vector $\tilde{P}$ depends nonlinearly upon the local value of the electric field strength $\tilde{E}$.

The process devices the optical wave equation in the usual manner by taking the curl $-\tilde{E}$ Maxwell equation (3.3) interchanged with the order of space and time derivative on the right-hand side of the resulting equation and uses equations (3.4), (3.6), and (3.7) to replace $\nabla \times \tilde{B}$ by $(1/c)\left(\partial \tilde{D}/\partial t\right)$ and obtain the equation.

$$\nabla \times \nabla \times \tilde{E} + \frac{1}{c^2}\frac{\partial^2 \tilde{D}}{\partial t^2} = 0 \tag{3.9a}$$

Use equation (3.8) to eliminate $\tilde{D}$ from this equation, and thereby obtain the expression.

$$\nabla \times \nabla \times \tilde{E} + \frac{1}{c^2}\frac{\partial^2}{\partial t^2}\tilde{E} = -\frac{4\pi}{c^2}\frac{\partial^2 \tilde{P}}{\partial t^2} \tag{3.9b}$$

This is the most general form of the wave equation in nonlinear optics. Under certain conditions it can be simplified. For example, by using an identity from vector calculus can write the first term on the left hand side of equation (3.9b) as

$$\nabla \times \nabla \times \tilde{E} = \nabla\left(\nabla \cdot \tilde{E}\right) - \nabla^2 \tilde{E} \tag{3.10}$$

In the linear optics of isotropic source free media, the first term on the right hand side of this equation vanishes because the Maxwell equation $\nabla \cdot \tilde{D} = 0$ implies $\nabla \cdot \tilde{E} = 0$. However, in nonlinear optics this term is generally non-vanishing even for isotropic materials, as a consequence of the more general relation (3.8) between $\tilde{D}$ and $\tilde{E}$. Fortunately, in nonlinear optics the first term on the right hand side of equation(3.10) can usually be dropped for cases of interest. For example, if $\tilde{E}$ is the form of a transverse, infinite plane wave, $\nabla \cdot \tilde{E}$ vanishes identically. More generally, the first term can often be shown to be small, even when it does not vanish identically, especially when the slowly varying amplitude approximation is valid. Assumedly, the contribution of $\nabla\left(\nabla \cdot \tilde{E}\right)$ in equation(3.10) is negligible so that the wave equation can be taken to have the form.

$$-\nabla^2 \tilde{\mathrm{E}} + \frac{1}{c^2}\frac{\partial^2 \tilde{\mathrm{E}}}{\partial t^2} = -\frac{4\pi}{c^2}\frac{\partial^2 \tilde{\mathrm{P}}}{\partial t^2} \tag{3.11}$$

where the polarization $\tilde{\mathrm{P}}$ characterizes the medium and it is a function of the electric field. In the case of weak nonlinear behavior of the medium, the polarization can be expressed by a Taylor polynomial as

$$\tilde{\mathrm{P}} = \underbrace{\varepsilon_0 \tilde{\mathrm{E}} + \varepsilon_0 \chi^{(1)} : \tilde{\mathrm{E}}}_{linear\ P_L} + \underbrace{\varepsilon_0 \chi^{(2)} :: \tilde{\mathrm{E}} \cdot \tilde{\mathrm{E}} + \varepsilon_0 \chi^{(3)} ::: \tilde{\mathrm{E}} \cdot \tilde{\mathrm{E}} \cdot \tilde{\mathrm{E}} + \ldots}_{nonlinear\ P_{NL}}, \quad (3.12)$$

where dielectric dispersion is ignored. $\chi^{(1)}$ is the linear susceptibility, represents the inner tensor product and the second and the third-order tensor $\chi^{(2)}$ and $\chi^{(3)}$ are responsible for the second harmonic generation, and the third-order harmonic generation respectively.

3.2 Nonlinear Refraction (Optical Kerr Effect)

The optical Kerr effect (i.e. nonlinear refraction index) results from the third order nonlinear susceptibility $\chi^{(3)}$, which is a fourth rank tensor. An optical wave is a real quantity and usually expressed as

$$\vec{\mathrm{E}}(t) = \mathrm{Re}\left\{\tilde{\mathrm{E}} \exp j(\vec{k} \cdot \vec{r} + \omega t)\right\} \quad (3.13)$$

or similarly as

$$\vec{\mathrm{E}}(t) = \frac{1}{2}\tilde{\mathrm{E}} \exp j(\vec{k} \cdot \vec{r} + \omega t) + c.c. \quad (3.14)$$

where *c.c.* represents the complex conjugate of the preceding term. Thus, an x-polarized optical wave, propagating in the z-direction in an isotropic medium, is represented mathematically as

$$\vec{\mathrm{E}}(t) = \frac{1}{2}\mathrm{E}_x \hat{x} \exp j(kz + \omega t) + c.c. \quad (3.15)$$

The third order polarization (mediated by $\chi^{(3)}$) in a material leads to a nonlinear intensity dependent contribution to its refractive index, i.e., the refractive index of the material changes as the incident intensity on the material changes. The susceptibility tensors in isotropic material can be further simplified as $\chi^{(2)} = 0$, due to inversion symmetry; the third order nonlinear susceptibility will only have one contributing term χ_{xxxx} since the light is x-polarized, and there are no means for sourcing additional polarization components.

The linear and nonlinear induced polarizations are

$$P_L = \varepsilon_0 (1 + \chi^{(1)}) E \quad (3.16)$$

and

$$\begin{aligned} P_{NL} &= P^{(3)} \\ &= \varepsilon_0 \chi_{xxxx}(\omega;-\omega,\omega,\omega)E^*EE \\ &\quad + \varepsilon_0 \chi_{xxxx}(\omega;\omega,-\omega,\omega)EE^*E \\ &\quad + \varepsilon_0 \chi_{xxxx}(\omega;\omega,\omega,-\omega)EEE^* \\ &= 3\varepsilon_0 \chi_{xxxx}|E|^2 E \\ &= \frac{3}{4}\varepsilon_0 \chi_{xxxx}|E_x|^2 E \end{aligned} \tag{3.17}$$

so that

$$P = P_L + P_{NL} = \varepsilon_0\left(1 + \chi^{(1)} + \frac{3}{4}\varepsilon_0 \chi_{xxxx}|E_x|^2\right)E$$

The total dielectric constant is

$$\varepsilon_r^{tot} = \varepsilon_r + \Delta\varepsilon_r$$

where $\varepsilon_r = 1 + \chi^{(1)} = n_o^2$ and $\Delta\varepsilon = \frac{3}{4}\chi_{xxxx}|E_x|^2$ after comparing with the expression for P.

The refractive index is related to the dielectric constant as:

$$n = \sqrt{\varepsilon_r + \Delta\varepsilon_r} \approx \sqrt{\varepsilon_r} + \frac{\Delta\varepsilon_r}{2\sqrt{\varepsilon_r}} = n_0 + \frac{3\chi_{xxxx}}{8n_0}|E_x|^2 \tag{3.18}$$

The intensity dependent refractive index for a nonlinear material is given by

$$n = n_0 + n_2|E|^2 \tag{3.19}$$

By comparing equations (3.8) and (3.9), the nonlinear refractive index is directly determined by the third-order susceptibility as

$$n_2 = \frac{3\chi_{xxxx}}{8n_0} = \frac{3\chi^{(3)}}{8n_0} \tag{3.20}$$

which characterizes the strength of the optical nonlinearity. The intensity *I* of an optical wave is proportional to $|E|^2$ as $I = \frac{1}{2\eta}|E|^2$ where η is the impedance of the medium. With comparing the optical response in the same medium, $I = |E|^2$ is taken for simplification.

3.3. Microring Resonator

A single ring resonator [44] is transferred into a box like filter shape using a single coupler or a double coupler configuration as shown in figures 3.1 and 3.4. A calculation model is derived, and all essential parameters describing the transmission characteristic are extracted in this section.

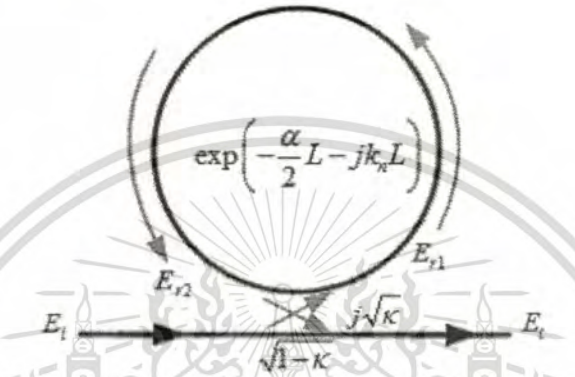

Figure. 3.1 Microring resonator.

The transfer function of this configuration is derived using Z-transform analysis. The circumference of the ring is L ($L = 2\pi R$, the radius is R); the coupling coefficient of the coupler is κ. The Z-transform parameter is represented by $z^{-1} = e^{-jk_n L}$ where $k_n = (2\pi/\lambda) n_{eff}$ is the propagation constant, and n_{eff} is the effective index of the waveguide. The one round trip loss is $a = e^{-\alpha L/2}$, α is the intensity attenuation coefficient inside the waveguide [unit $length^{-1}$]. The transmitted or throughput field at the output of the straight waveguide E_t and inserted electric field E_i relations can be derived as followed and from shown in figure. 3.1.

where

E_i the incoming light field of an input port

E_t the transmitted light field to the output port

L the circumference of the fiber ring ($L = 2\pi R$, R is the radius)

κ the coupling coefficient of the coupler

α the intensity attenuation coefficient

k_n the Wave propagation constant

Here, the input light is assumed to be monochromatic with constant amplitude and random phase modulation which results in temporal coherence degradation. Therefore, the input light field can be expressed as

$$E_i = E_0 \cdot e^{(j \cdot \phi_0)}$$

According to the light pulse is input and propagated within a fiber ring resonator, obtained the relations between the electric fields E_{r1}, E_{r2}, E_t and the output field E_i as following equations:

$$E_t = \sqrt{1-\gamma} \cdot \left[E_i \cdot \sqrt{1-\kappa} + j \cdot E_{r2} \sqrt{\kappa} \right] \tag{3.21}$$

$$E_{r1} = \sqrt{1-\gamma} \cdot \left[j \cdot E_i \cdot \sqrt{\kappa} + E_{r2} \cdot \sqrt{1-\kappa} \right] \tag{3.22}$$

$$E_{r2} = E_{r1} \cdot e^{\left(-\frac{\alpha}{2} \cdot L - j \cdot k_n \cdot L \right)} \tag{3.23}$$

where

γ is the intensity insertion loss coefficient of the directional coupler.

E_{r1} and E_{r2} are the circulated fields inside the fiber.

Replace equation (3.23) into equation (3.22)

$$E_{r1} = \frac{\sqrt{1-\gamma} \cdot j \cdot E_i \cdot \sqrt{\kappa}}{1 - \sqrt{1-\gamma} \cdot e^{\left(-\frac{\alpha}{2} \cdot L - j \cdot k_n \cdot L \right)} \cdot \sqrt{1-\kappa}} \tag{3.24}$$

and institute equation (3.24) into equation (3.23), so that

$$E_{r2} = \frac{\sqrt{1-\gamma} \cdot j \cdot E_i \cdot \sqrt{\kappa}}{1 - \sqrt{1-\gamma} \cdot e^{\left(-\frac{\alpha}{2} \cdot L - j \cdot k_n \cdot L \right)} \cdot \sqrt{1-\kappa}} \cdot e^{\left(-\frac{\alpha}{2} \cdot L - j \cdot k_n \cdot L \right)} \tag{3.25}$$

Then replace equation (3.25) into equation (3.21).

$$E_t = \left[\sqrt{1-\gamma} \cdot \left(\frac{\sqrt{1-\kappa} - \sqrt{1-\gamma} \cdot e^{\left(-\frac{\alpha}{2}L - jk_nL\right)}}{1 - \sqrt{1-\gamma} \cdot e^{\left(-\frac{\alpha}{2}L - jk_nL\right)} \cdot \sqrt{1-\kappa}} \right) \right] E_i \tag{3.26}$$

Using equation (3.26), E_t / E_i or E_{out} / E_{in} can be calculated as

$$\frac{E_{out}}{E_{in}} = \left[\sqrt{1-\gamma} \cdot \left(\frac{\sqrt{1-\kappa} - \sqrt{1-\gamma} \cdot e^{\left(-\frac{\alpha}{2}L - jk_nL\right)}}{1 - \sqrt{1-\gamma} \cdot e^{\left(-\frac{\alpha}{2}L - jk_nL\right)} \cdot \sqrt{1-\kappa}} \right) \right] \tag{3.27}$$

From equation (3.27), $I_{out}/I_{in} = |E_{out}|^2 / |E_{in}|^2$;

$$\left|\frac{E_{out}}{E_{in}}\right|^2 = \left(\sqrt{1-\gamma} \cdot \left[\frac{\sqrt{1-\kappa} - \sqrt{1-\gamma} \cdot e^{\left(-\frac{\alpha}{2}L - jk_nL\right)}}{1 - \sqrt{1-\gamma} \cdot e^{\left(-\frac{\alpha}{2}L - jk_nL\right)} \cdot \sqrt{1-\kappa}} \right] \right) \left(\sqrt{1-\gamma} \cdot \left[\frac{\sqrt{1-\kappa} - \sqrt{1-\gamma} \cdot e^{\left(-\frac{\alpha}{2}L - jk_nL\right)}}{1 - \sqrt{1-\gamma} \cdot e^{\left(-\frac{\alpha}{2}L - jk_nL\right)} \cdot \sqrt{1-\kappa}} \right] \right) \tag{3.28}$$

or

$$\frac{I_o}{I_i} = \left| \frac{E_{out}(t)}{E_{in}(t)} \right|^2$$

$$= (1-\gamma) \left[1 - \frac{\left(1 - (1-\gamma)x^2\right)\kappa}{\left(1 - x\sqrt{1-\gamma}\sqrt{1-\kappa}\right)^2 + 4x\sqrt{1-\gamma}\sqrt{1-\kappa}\sin^2\left(\frac{\phi}{2}\right)} \right] \tag{3.29}$$

The transfer function in equation (3.29) indicates that a ring resonator is very similar to a Fabry-Perot cavity. In the particular case shown in figure 3.1, the corresponding Fabry-Perot cavity would have an input mirror with a field reflectivity and a fully reflecting output mirror. However, the field propagating inside the ring cavity is a traveling wave in contrast to the Fabry-Perot cavity which resonates a standing wave.

3.3.1 Bistability Phenomenon

The phenomenon of Optical Bistability (OB) is the nonlinear phenomenon of microring resonator [45] arises from a combination of the nonlinearity in the radiation-matter interaction and of a feedback mechanism [37-39]. Generally, there are two classes of OB: absorptive and dispersive OB.

Absorptive OB occurs whenever the input wavelength is closed to the atomic resonance of the material. An increase in the input power produces the increasing in saturation, i.e. in the degree of transparency of the medium. This allows the internal field of the cavity to increase and in return increases the saturation. Such positive feedback loop causes the switch-up process. Moreover, when the input power is decreased, the internal field is intense enough to maintain the saturation. As a consequence, the transmitted power is held "ON" and one obtains a hysteresis curve. **InGaAsP** can be designed to have the band edge around 1.45 μm and thus can show absorptive OB when it is pumped at 1.55 μm. On the other hand, dispersive OB occurs whenever the input wavelength is tuned far away from the atomic resonance and hence the material is transparent. The frequency of the incident field is kept near one of the cavity frequencies, but detuned enough so that the transmission is low. An increase in the input intensity produces an increase in the intensity of the internal field. Because the refractive index is a function of intensity, this changes the optical length of the medium in such a way that the cavity resonance is driven closer to the input frequency. Therefore, it increases the internal field intensity. Thus, again, we have a positive feedback loop which produces up-switching. When the incident power is decreased, the internal field is intense enough to maintain resonance between the cavity and the input frequency, so one again obtains a hysteresis which the input wavelength is at 1.55 μm. The characteristic of bistability hysteresis can be implemented as optical switching.

3.2.2 Bifurcation Phenomenon

Bifurcation theory is the mathematical study of how and when the solution to a problem changes from only being one possible to there being two solitons, which is called a bifurcation. In most commonly used in the mathematical study of dynamical systems, a bifurcation occurs when a small smooth change made to the parameter values (the bifurcation parameters) of a system causes a sudden "qualitative" or topological change in its long-term dynamical behavior. Bifurcations occur in both continuous systems and discrete systems [40, 41].

The study of how the character of fixed points change as parameters of the system change is called "bifurcation theory" (Recall that the term bifurcation is used to describe any sudden changes in the dynamics of the system. When a fixed point changes character as parameter values change, the behavior of trajectories in the neighborhood of that fixed point will change. Hence, the term bifurcation is appropriate here.) Being able to classify and understand the various possible bifurcations is an important part of the study of nonlinear dynamics.

3.3.3 Chaotic Phenomenon

Optical Chaos are observed in many nonlinear optical systems. One of the most common example is a ring resonator, and One of the most seminal works is published by Ikeda (Physical Review Letters, 1982), which chaotic behavior in a ring resonator was proposed and experimentally confirmed. Optical Chaos was an exciting field of research in mid-1980s and was expected at that time to lead to production of all optical devices including all optical computers. Researchers realized later that the inherent limitation of the optical systems is due to the non-localized nature of photons compared to highly localized nature of electrons. Research in Optical Chaos has seen a recent resurgence in the context of studying synchronization phenomena and developing techniques for secure optical communications. [33, 34]

3.4 Chaos in Communication

The appearance in the year of 1990 of two seminal papers involving fundamentals of chaotic systems generated a tremendous amount of interest and work with subsequent applications in synchronization and control of chaos. Particularly, the peculiar features of chaotic systems well explored [44] (synchronization capability) and (sensitivity to initial condition) [45] opened up a whole new field for using chaotic signals as information carriers. It is currently accepted that chaotic systems provide a rich mechanism for signal design and generation with promising potential applications to communications and signal processing. Since chaotic signals are typically broadband, noise-like, and difficult to predict, they can be used in various contexts for masking information-bearing waveforms. They can also be used as modulating waveforms in spread spectrum systems, like Code Division Multiple Access (CDMA) that is becoming very popular in many fields of telecommunication. Two fundamental characteristics of chaos in physical systems are the complexity of the dynamics and the sensitivity of the time evolution to small perturbations. The sensitivity of chaos to small perturbations has been seen for a long time as merely a barrier to prediction and not as a useful property.

Major developments in the area of controlling chaos using small perturbations have proved; otherwise, the sensitivity to small perturbations exhibited by chaotic systems allows controlling them using.chaos communication is an application of chaos theory which is aimed to provide security in the transmission of information performed through telecommunications technologies. By securing communications, one has to understand that the contents of the message transmitted are inaccessible to possible eavesdroppers.

Chaos communication security (i.e., privacy) is based on the complex dynamic behaviors provided by chaotic systems. Some properties of chaotic dynamics, such as complex behaviors, noise-like dynamics (pseudorandom noise), and spread spectrum are used to encode data. On the other hand, being chaos a deterministic phenomenon it is possible to decode data using this determinism. In practice, implementations of chaos communication devices resort to one of two chaotic phenomena: synchronization of chaos or control of chaos. The implement chaos communications using such properties of chaos, two chaotic oscillators are required as a transmitter (master) and receiver (slave). In the transmitter, a message is added on to a chaotic signal and then, the message is masked in the chaotic signal. As it carries the information, the chaotic signal is also called chaotic carrier.

When chaos synchronization is used, a basic scheme of a communication device (Cuomo and Oppenheim 1993) is made by two identical chaotic oscillators. One of them is used as the transmitter and the other as the receiver. They are connected in a configuration where the transmitter drives the receiver in such a way that identical synchronization of chaos between the two oscillators is achieved. For the purpose of transmission of information, at the transmitter, a message is added as a small perturbation to the chaotic signal that drives the receiver. In this way, the message transmitted is masked by the chaotic signal. When the receiver synchronizes to the transmitter, the message is decoded by a subtraction between the signal sent by transmitter and its copy generated at the receiver by means of the synchronization of chaos mechanism. This works because while the transmitter output contains the chaotic carrier plus the message, the receiver output is made only by a copy of the chaotic carrier without the message. The electrical signals with a power are produced by the chaotic system itself. Thus, the complexity of chaos and its sensitivity to small perturbations can be combined harmoniously by using the sensitivity to control (and take advantage of) the complexity.

As a consequence, it is currently recognized by many engineers that in the fact chaos that provides complex behavior from simple systems can be exploited to obtain technological advantages over conventional means for information transmission. To design the nonlinear microring resonator, the nonlinear behaviors of light in ring is firstly, required to characterize. The nonlinear of the microring resonator with the input is the soliton pulse as shown in figure 3.2.The wave form of the soliton pulse is used as input signal with pulse width of 50 ps shown in figure 3.2 (a), which is the input into nonlinear microring. While figure 3.2 (b) shows the output signal generated from the microring resonator due to Kerr effect, the chaotic wave form is realized. Here, the radius of the ring is set equal 10 μm.

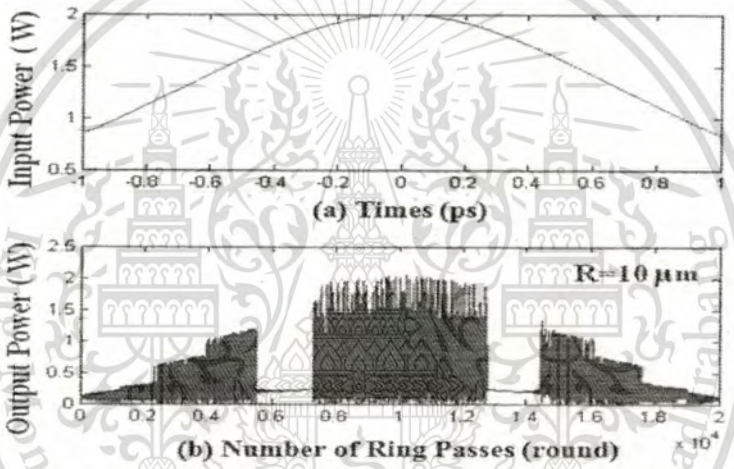

Figure 3.2 Shows the soliton pulse input and the chaotic signal output generated from microring resonator.

The characteristics of the chaotic signal output by varying the intense of input powers are shown in figure 3.3. The input powers in figure 3.3 (a)-(d) are set power 2, 3, 4, and 5 W, respectively. The result in figure 3.3 (a), the chaotic behavior is seen when the roundtrips of input soliton are in the range of 9,000-11,000. Similarly, in figures. 3.3 (b)-3.3 (d) with the input peak powers 3-5 W, the chaotic signals are occurred when the soliton is circulated within the ring between 8,000-12,500 roundtrips.

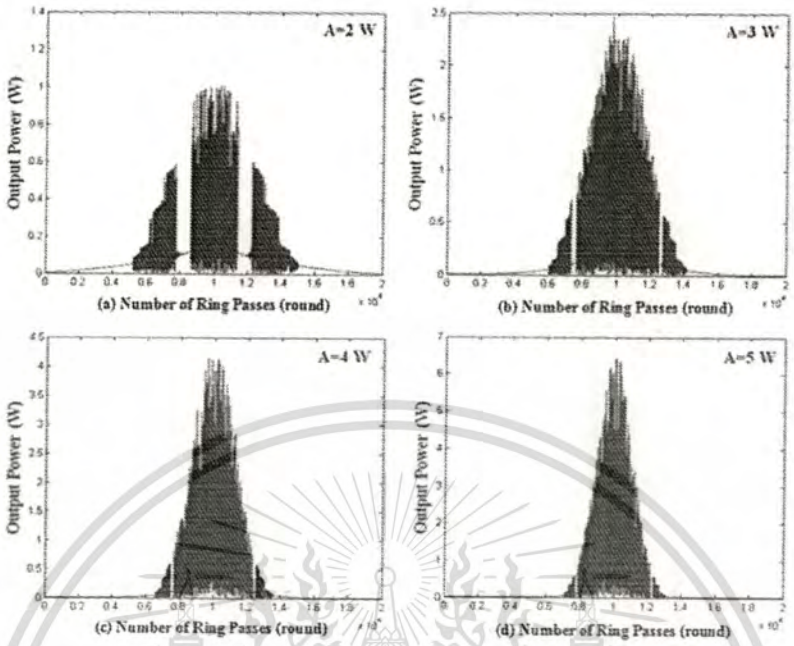

Figure 3.3 Shows the generation of chaotic signal by varying input peak powers (w), (a) 2 W, (b) 3 W, (c) 4 W, and (d) 5 W.

On figure 3.4 shows the generation of chaotic signal with different ring radii. figure 3.4 (a), the soliton chaotic behavior is occurred with mostly constant output intensity; the roundtrips are in the range of 6,000-14,000, and the ring radius is 7 μm. When the ring radius is adjusted as 10 μm, we found that the soliton chaotic is realized with the roundtrips between 7,800-12,800 as show in the figure. 3.4(b). In figure3.4(c) and (d), the results of the different ring radii of 12 μm and 15 μm have shown that the soliton chaotic behaviors are seen with the roundtrips between 4,500-15,500 and 2,300-17,500 respectively.

Results of the different coupling coefficients from 0.1-0.4 are shown in figure 3.5 However, figure 3.5 (a) and figure 3.5 (b) show that the soliton chaotic behaviors with the roundtrips between 4,500-15,500 and 6,100-14,000 with the coupling coefficients are 0.1 and 0.2 respectively while figures 3.5 (c) and (d) with the coupling coefficient 0.3 and 0.4 show the soliton chaotic behaviors with the roundtrips between 9,500-11,500 and 1,000-19,000.

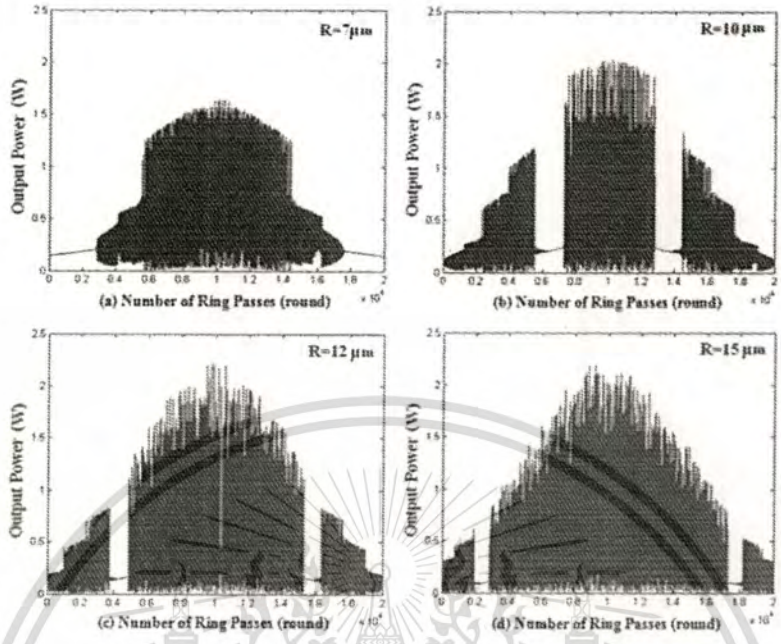

Figure 3.4 Shows the generation of chaotic signal by varying ring radii of ring resonator, (a) 7 μm, (b) 10 μm, (c) 12 μm, and (d) 15 μm.

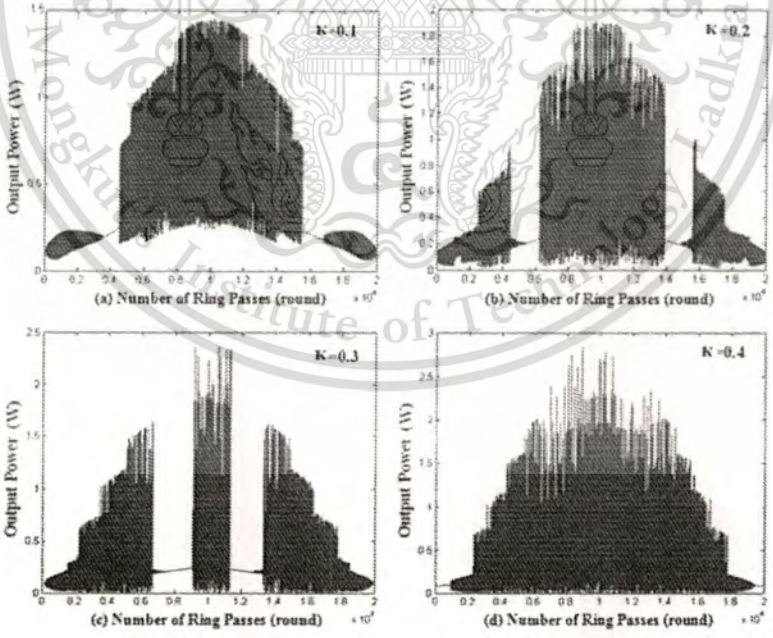

Figure. 3.5 Shows the generation of chaotic signal by varying couple coefficient (κ), (a) $\kappa = 0.1$, (b) $\kappa = 0.2$, (c) $\kappa = 0.3$, and (d) $\kappa = 0.4$.

3.5 .Add Drop Filter

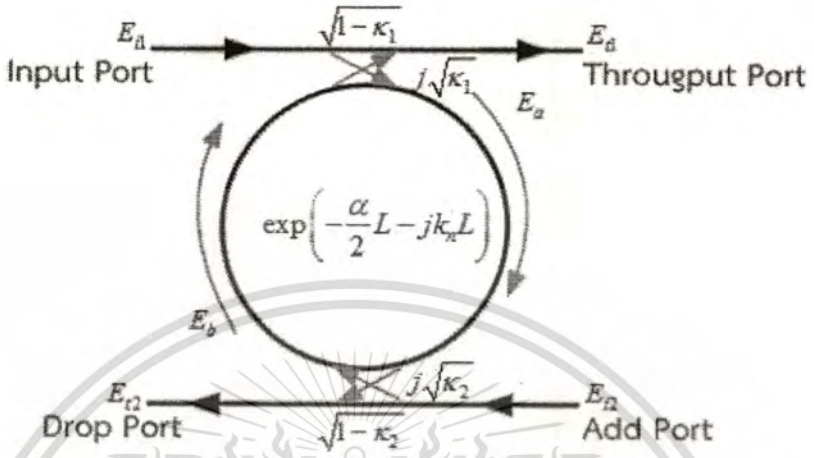

Figure 3.6 Add/Drop Filter

For simplification, the calculation of the intensity relation does not take into account coupling losses $(\gamma = 0)$ that is $\left(\sqrt{1-\gamma}\right)^2 = 1$.

The relationship of the input electric transmission and electric field are as follows:

E_{i1} the input field

E_{t1} the throughput field

E_{t2} the dropped field

E_a and E_b are the fields in the ring

κ_1 the field coupling coefficient between the input bus and the ring

κ_2 the field coupling coefficient between the ring and the input bus

L the circumference of the ring

Theoretical transmission (Light Transmission Theory) is the relationship between electric field E_a and E_b within the ring $\frac{L}{2}$.

$$E_a = E_{i1} j\sqrt{\kappa_1} + E_b \sqrt{1-\kappa_1} e^{-\frac{\alpha L}{2\,2} - jk_n \frac{L}{2}} \tag{3.30}$$

$$E_b = E_a \sqrt{1-\kappa_2} e^{-\frac{\alpha L}{2\,2} - jk_n \frac{L}{2}} \tag{3.31}$$

The relationship between electric field E_b and E_a is equation (3.32).

$$E_a = \frac{E_{i1} j\sqrt{\kappa_1}}{1-\sqrt{1-\kappa_1}\sqrt{1-\kappa_2}\,e^{-\frac{\alpha}{2}L-jk_nL}} \tag{3.32}$$

$$E_b = \frac{E_{t1} j\sqrt{\kappa_1}}{1-\sqrt{1-\kappa_1}\sqrt{1-\kappa_2}\,e^{-\frac{\alpha}{2}L-jk_nL}} \cdot \sqrt{1-\kappa_2}\,e^{-\frac{\alpha L}{2\,2}-jk_n\frac{L}{2}} \tag{3.33}$$

$$E_{t1} = E_b e^{-\frac{\alpha L}{2\,2}-jk_n\frac{L}{2}} j\sqrt{\kappa_1} + E_{i1}\sqrt{1-\kappa_1} \tag{3.34}$$

$$E_{t2} = E_a e^{-\frac{\alpha L}{2\,2}-jk_n\frac{L}{2}} j\sqrt{\kappa_2} \tag{3.35}$$

when $E_{t2} = 0$

$$E_1 = \frac{E_{i1} j\sqrt{1-\gamma_1}\sqrt{\kappa_1}}{1-\sqrt{1-\gamma_1}\sqrt{1-\kappa_1}\sqrt{1-\gamma_2}\sqrt{1-\kappa_2}\,e^{-\frac{\alpha}{2}L-jk_nL}} \tag{3.36}$$

$$\frac{E_{t1}}{E_{i1}} = \frac{-\sqrt{1-\kappa_2}\,e^{-\frac{\alpha}{2}L-jk_nL}+\sqrt{1-\kappa_1}}{1-\sqrt{1-\kappa_1}\sqrt{1-\kappa_2}\,e^{-\frac{\alpha}{2}L-jk_nL}} \tag{3.37}$$

$$\frac{E_{t2}}{E_{i1}} = \frac{-\sqrt{\kappa_1\cdot\kappa_2}\,e^{-\frac{\alpha L}{2\,2}-jk_n\frac{L}{2}}}{1-\sqrt{1-\kappa_1}\sqrt{1-\kappa_2}\,e^{-\frac{\alpha}{2}L-jk_nL}} \tag{3.38}$$

By using the upper equations, the transfer function for throughput port and drop port in figure 3.12 can be expressed as the intensity relations for the throughput and drop port can be obtained by normalizing the transfer functions in equations. (3.39) and (3.40) which are given by

Throughput port:

$$\frac{I_t}{I_i} = \left|\frac{E_t}{E_{in}}\right|^2 = \left[\frac{(1-\kappa_1)-2\sqrt{1+\kappa_1}\cdot\sqrt{1-\kappa_2}\,e^{-\alpha/2L}\cos(k_nL)+(1-\kappa_2)e^{-\alpha L}}{1+(1-\kappa_1)(1-\kappa_2)e^{-\alpha L}-2\sqrt{1-\kappa_1}\cdot\sqrt{1-\kappa_2}\,e^{-\alpha/2L}\cos(k_nL)}\right] \tag{3.30}$$

Drop port:

$$\frac{I_d}{I_i} = \left|\frac{E_d}{E_{in}}\right|^2 = \left[\frac{\kappa_1\kappa_2 e^{-\alpha/2L}}{1+(1-\kappa_1)(1-\kappa_2)e^{-\alpha L}-2\sqrt{1-\kappa_1}\cdot\sqrt{1-\kappa_2}\,e^{-\alpha/2L}\cos(k_nL)}\right] \tag{3.40}$$

The outputs intensity I_t and I_d at the throughput and drop port from equations (3.39) and (3.40) will be zero at resonance $k_n L = 2m\pi$,which indicates that the resonance wavelength is fully extracted by the resonator for identical symmetrical codirectional couplers $\kappa_1 = \kappa_2$ if $\alpha = 0$ as shown in figure 3.7.

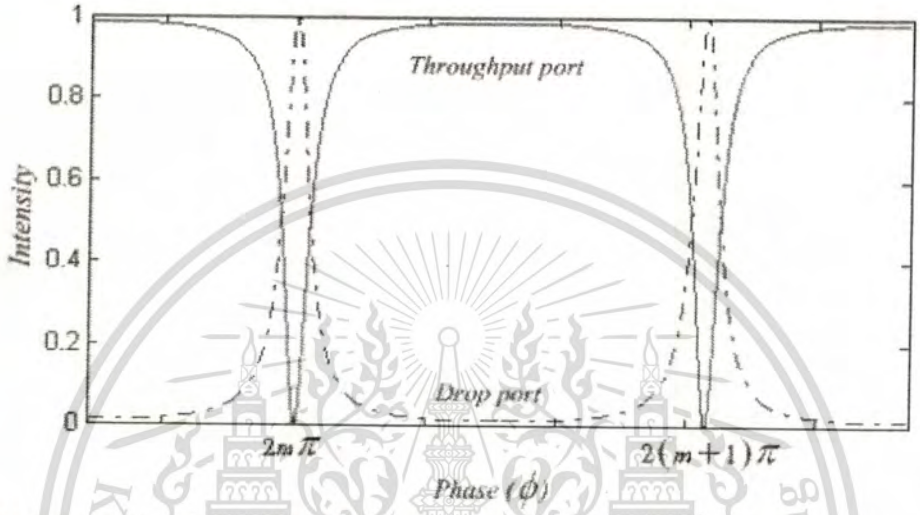

Figure 3.7 Simulation data of the filtering responses of the Add/Drop filter with $\kappa_1 = \kappa_2 = 0.2$, $\alpha = 0, \gamma = 0$, R = 150 μm.

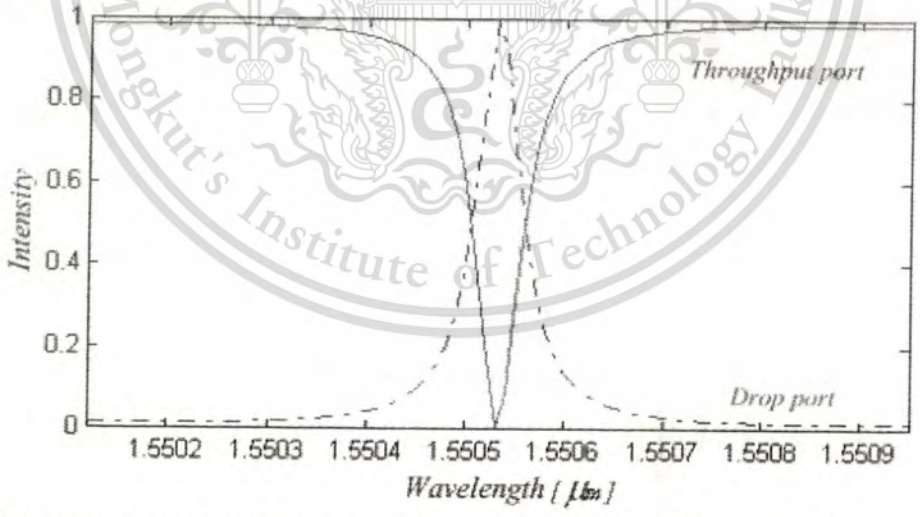

Figure 3.8 Transmission characteristic of the Add/Drop filter with $\kappa_1 = \kappa_2 = 0.2$, $\alpha = 0$, $\gamma = 0$, R = 150 μm.

The filter characteristics as shown in figure 3.7 are the simulation results of the throughput and drop port of the Add/Drop filter as figure 3.8. The Add/Drop filter has a radius equal to 150 μm with the coupling coefficients of $\kappa_1 = \kappa_2 =$ 0.2. The refractive index is assumed to be 3.5, and the internal loss are fully compensated ($\alpha = 0$) by using the Add/Drop filter with a low coupling coefficients of $\kappa_1 = \kappa_2 =$ 0.2, for identical symmetrical codirectional couplers. Finally, The communication application by using the proposed device in this chapter introduces the nonlinear equation and simple overview of nonlinear phenomenal. The next chapter goes into detail with the most important nonlinearities in microring resonator communication systems.

CHAPTER 4

NARROW SPECTRAL WIDTH GENERATION BASED ON NONLINEAR MULTI-STEP MICRORING RESONATORS

In this chapter, the interesting results of high frequency generation method which is required to use in the THz regime is presented. A system consists of a serial nonlinear microring resonator system for generating pulse and selecting signals that can be filtered by using the Add/Drop filter. By controlling the ring parameters, the appropriate output power can be obtained and modified to be suitable in either network or communication applications. Moreover, the very wide band of wavelength can be generated and controlled for various applications. The organization of chapter comprise of operating principle simulation results, operating principle, multi wavelength generation result, multi frequency generation result, and microring resonator characterize evaluation using Optiwave FDTD method.

4.1 Operating Principle

Light from a monochromatic light source is launched into a ring resonator with constant light field amplitude (E_0) and random phase modulation as shown in figure 4.1 which is the combination terms in attenuation (α) and phase (ω_o) constants resulting in temporal coherence degradation. Therefore, the time dependent input light field (E_{in}) without pumping term can be expressed as [46] :

$$E_{in}(t) = E_0 e^{-\alpha L + j\phi_0(t)} \tag{4.1}$$

Where

L is a propagation distance(waveguide length).

By the assumption nonlinearity of nonlinear microring resonator is of the Kerr effect, i.e. the refractive index is given by

$$n = n_0 + n_2 I = n_0 + n_2 \left(P / A_{eff} \right) \tag{4.2}$$

Where

n_0 is the linear refractive indexes.

n_2 is the nonlinear refractive indexes.

I is the optical intensity.

P is the optical power.

A_{eff} is the effective mode core area of the device.

For the microring resonators, the effective mode core areas are range from 0.10 to 0.50 μm^2 [47].When a Gaussian pulse is input and propagated within a fiber ring resonator, the resonant output is formed, thus, the normalized output of the light field is the ratio between the output fields ($E_{out}(t)$) and input fields ($E_{in}(t)$) in each roundtrip, which can be expressed as [48].

$$\left|\frac{E_{out}(t)}{E_{in}(t)}\right|^2 = (1-\gamma)\left[1 - \frac{\left(1-(1-\gamma)x^2\right)\kappa}{\left(1-x\sqrt{1-\gamma}\sqrt{1-\kappa}\right)^2 + 4x\sqrt{1-\gamma}\sqrt{1-\kappa}\sin^2(\phi/2)}\right] \tag{4.3}$$

From equation (4.3) indicates that a ring resonator in the particular case is very similar to a Fabry-Perot cavity which has an input and output mirror with a field reflectivity $(1-\kappa)$ and a fully reflecting mirror. κ is the coupling coefficient and $x = e^{(-\alpha L/2)}$ represents a roundtrip loss coefficient, $\phi_0 = kLn_0$ and $\phi_{NL} = kL\left(n_2 / A_{eff}\right)$ is the linear and nonlinear phase shifts; $k = 2\pi/\lambda$ is the wave propagation number in a vacuum, L and α respectively are a waveguide length and linear absorption coefficient. In this work, the iterative method is introduced to obtain the results as shown in equation (4.3) from figure 4.1 (a). Likewise, the output field is connected and input into the other ring resonators.

Throughput port:

$$\left|\frac{E_t}{E_{in}}\right|^2 = \left[\frac{(1-\kappa_1) - 2\sqrt{1+\kappa_1}\cdot\sqrt{1-\kappa_2}e^{-\alpha/2L}\cos(k_nL) + (1-\kappa_2)e^{-\alpha L}}{1+(1-\kappa_1)(1-\kappa_2)e^{-\alpha L} - 2\sqrt{1-\kappa_1}\cdot\sqrt{1-\kappa_2}e^{-\alpha/2L}\cos(k_nL)}\right] \tag{4.4}$$

Drop port:

$$\left|\frac{E_d}{E_{in}}\right|^2 = \left[\frac{\kappa_1\kappa_2 e^{-\alpha/2L}}{1+(1-\kappa_1)(1-\kappa_2)e^{-\alpha L} - 2\sqrt{1-\kappa_1}\cdot\sqrt{1-\kappa_2}e^{-\alpha/2L}\cos(k_nL)}\right] \tag{4.5}$$

A Gaussian pulse the input optical field as shown in equation (4.1) is fed input into a nonlinear microring resonator. By using the appropriate parameters, the chaotic signal is obtained by equation (4.3). To retrieve the signals from the chaotic noise, the Add/Drop device with the appropriate parameters is used by following details. The optical outputs of a ring resonator Add/Drop filter is given via the equations (4.4) and (4.5) from figure 4.1 (b), then E_t and E_d represent the optical fields of the throughput and drop ports. The transmitted output can be controlled and obtained by choosing the suitable coupling ratio of the ring resonator, which is well derived and described by reference [49]. Where $\beta = kn_{eff}$ represents the propagation constant,

n_{eff} is the effective refractive index of the waveguide, the circumference of the ring is $L = 2\pi R$, and R is the radius of the ring. In the following, new parameters will be used for simplification, $\phi = \beta L$ is the phase constant. The chaotic noise cancellation is managed by using the specific parameters of the Add/Drop device, which require signals at the specific wavelength band can be filtered and retrieved κ_1 and κ_2 are coupling coefficient of Add/Drop filters, $k_n = 2\pi / \lambda$ is the wave propagation number for in a vacuum, and the waveguide (ring resonator) loss is α = 0.5 dB/mm, so the fractional coupler intensity loss is γ = 0.1.

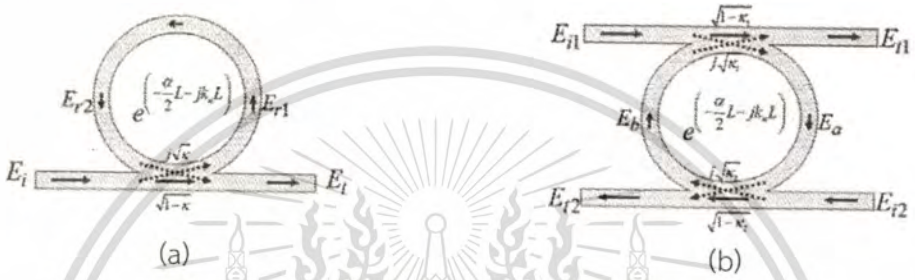

Figure 4.1 Schematic diagram of ring resonator.
(a) a microring resonator
(b) an Add/Drop filter

The frequency spacing between two resonance peaks is called the FSR which is calculated as followed [50] :

$$FSR = \Delta\lambda = \frac{\lambda_i^2}{n_{eff} L} \tag{4.6}$$

and

$$FSR = \Delta f = \frac{c}{n_{eff} L} \tag{4.7}$$

Here, n_{eff} is the effective refractive index and L is the circumference of the ring.

The FWHM $\left(\delta_\phi\right)$ in term of frequency and wavelength at the resonance peaks is given by

$$\delta_\phi = 2\frac{1 - y_1 y_2 x}{\sqrt{y_1 y_2 x}} \tag{4.8}$$

where

$$x = e^{\left(-\frac{\alpha}{2} \cdot L\right)}$$
$$y_1 = \sqrt{1-\kappa_1}$$
$$y_2 = \sqrt{1-\kappa_2}$$

The Finesse (F) is given by.

$$F = \frac{2\pi}{\delta_\phi} = \frac{\pi\sqrt{y_1 y_2 x}}{1 - y_1 y_2 x} \tag{4.9}$$

The FWHM of Wavelength (δ_λ)

$$FWHM = \delta\lambda = \frac{c}{F \cdot n_{eff} \cdot L} \tag{4.10}$$

and

The FWHM of Frequency (δ_f)

$$FWHM = \delta f = \frac{\lambda^2}{F \cdot n_{eff} \cdot L} \tag{4.11}$$

4.2 Simulation and Result

To design the nonlinear microring resonator, the nonlinear behaviors of light in ring are firstly required to characterize. The Gaussian pulse input power (E_{in}) with the frequency between 1400 to 1600 nm is shown in figure 4.2, which is the result of equation (4.1).

Figure 4.2 The input Gaussian pulse.

In figure 4.4. is the result from equation (4.12) when the ring radius (R_1) is $15\mu m$, and coupling coefficient (κ_1) is 0.89.

$$\left|E_{out}\right|^2 = \left|E_{in}\right|^2 \cdot \left[(1-\gamma)\left(1 - \frac{\left(1-(1-\gamma)x^2\right)\kappa}{\left(1 - x\sqrt{1-\gamma}\sqrt{1-\kappa}\right)^2 + 4x\sqrt{1-\gamma}\sqrt{1-\kappa}\sin^2\left(\frac{\phi}{2}\right)} \right) \right] \tag{4.12}$$

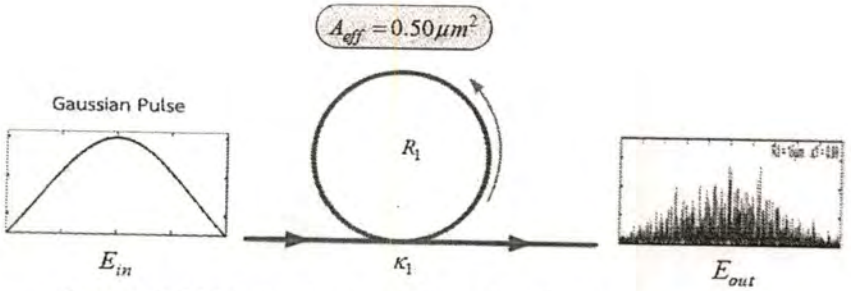

Figure 4.3 The nonlinear of the microring resonator (R_1).

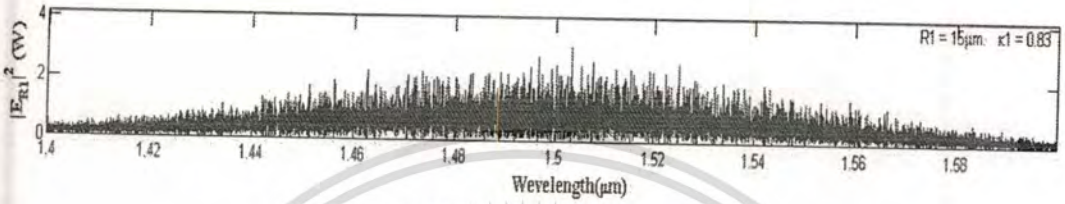

Figure 4.4 Large bandwidth signal.

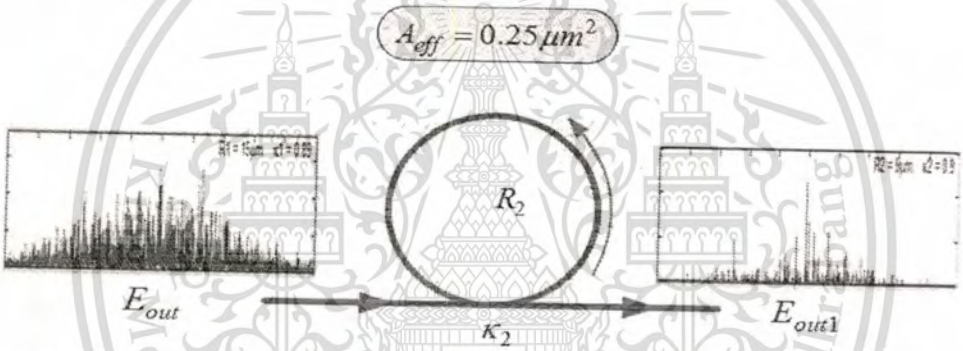

Figure 4.5 The nonlinear of the microring resonator (R_2).

When $E_{out} = E_{in}$ and $E_{out1} = E_{out}$;

$$\left|E_{out}\right|^2 = \left|E_{out1}\right|^2 \cdot \left[(1-\gamma)\left(1 - \frac{\left(1-(1-\gamma)x^2\right)\kappa}{\left(1-x\sqrt{1-\gamma}\sqrt{1-\kappa}\right)^2 + 4x\sqrt{1-\gamma}\sqrt{1-\kappa}\sin^2\left(\frac{\phi}{2}\right)} \right) \right] \quad (4.13)$$

From equation (4.13) the nonlinear of the microring resonator is shown in figures 4.5 and 4.6 when the ring radius (R_2) is $9\mu m$, and coupling coefficient (κ_2) is 0.89.

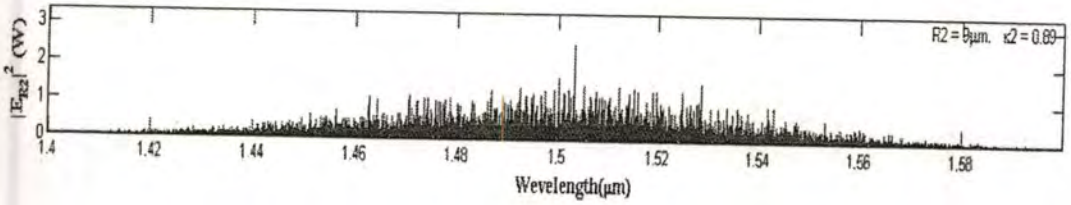

Figure 4.6 The filtering and amplifying signals.

$A_{eff} = 0.10\mu m^2$

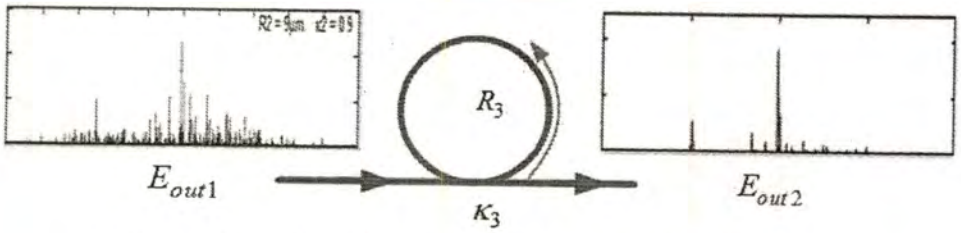

Figure 4.7 The nonlinear of the microring resonator (R_3).

When $E_{out1} = E_{in}$ and $E_{out2} = E_{out}$;

$$\left|E_{out2}\right|^2 = \left|E_{out1}\right|^2 \cdot \left[(1-\gamma)\left[1 - \frac{\left(1-(1-\gamma)x^2\right)\kappa}{\left(1-x\sqrt{1-\gamma}\sqrt{1-\kappa}\right)^2 + 4x\sqrt{1-\gamma}\sqrt{1-\kappa}\sin^2\left(\frac{\phi}{2}\right)} \right] \right] \quad (4.14)$$

From equation (4.14) the nonlinear of the microring resonator is shown in figures 4.7 and 4.8, when the ring radius (R_3) is $9\mu m$ and coupling coefficient (κ_3) is 0.96.

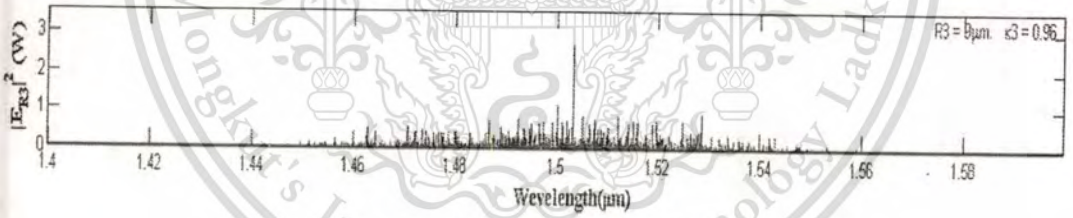

Figure 4.8 The storage unit.

$A_{eff} = 0.50\mu m^2$ $A_{eff} = 0.25\mu m^2$ $A_{eff} = 0.10\mu m^2$

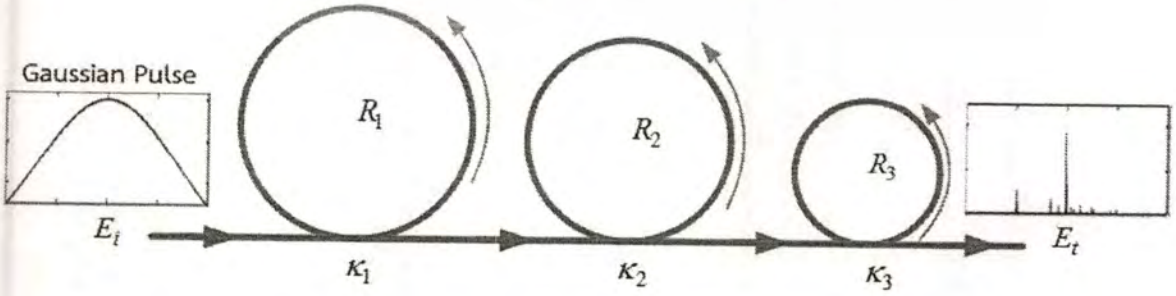

Figure 4.9 The nonlinear microring resonator system.

Figure 4.9 shows a series of nonlinear microring resonator (InGaAsP/InP) [51, 52]. The input signal is a Gaussian pulse (2w) and the effective mode core area of the fiber (A_{eff}) is 0.50μm^2, 0.25 μm^2 and 0.10 μm^2 by adjusting the parameters accordingly. In this thesis, nonlinear effects the optical fiber ring resonator such as chaos phenomenon studied by changing the optical parameters resulted in the optical output changing such as ring radii and chaos effects. The relation between those parameters and output powers are derived by varying parameters showing that the parameters of such a system can be changed, and the nonlinear effects characteristics can be controlled. The selected signals can be filtered by using the optical Add/Drop filter. By controlling the ring parameters, the appropriate output power can be obtained and modified to be suitable in either network or optical communication applications.

When $E_{out2} = E_{in}$, $E_d = E_{Drop\ port}$ and $E_t = E_{Througput\ port}$ are output electric fields.

$$|E_t|^2 = |E_{in}|^2 \cdot \left[\frac{(1-\kappa_1) - 2\sqrt{1+\kappa_1}\cdot\sqrt{1-\kappa_2}\,e^{-\alpha/2L}\cos(k_n L) + (1-\kappa_2)e^{-\alpha L}}{1+(1-\kappa_1)(1-\kappa_2)e^{-\alpha L} - 2\sqrt{1-\kappa_1}\cdot\sqrt{1-\kappa_2}\,e^{-\alpha/2L}\cos(k_n L)} \right] \quad (4.15)$$

and

$$|E_d|^2 = |E_{in}|^2 \cdot \left[\frac{\kappa_1\kappa_2 e^{-\alpha/2L}}{1+(1-\kappa_1)(1-\kappa_2)e^{-\alpha L} - 2\sqrt{1-\kappa_1}\cdot\sqrt{1-\kappa_2}\,e^{-\alpha/2L}\cos(k_n L)} \right] \quad (4.16)$$

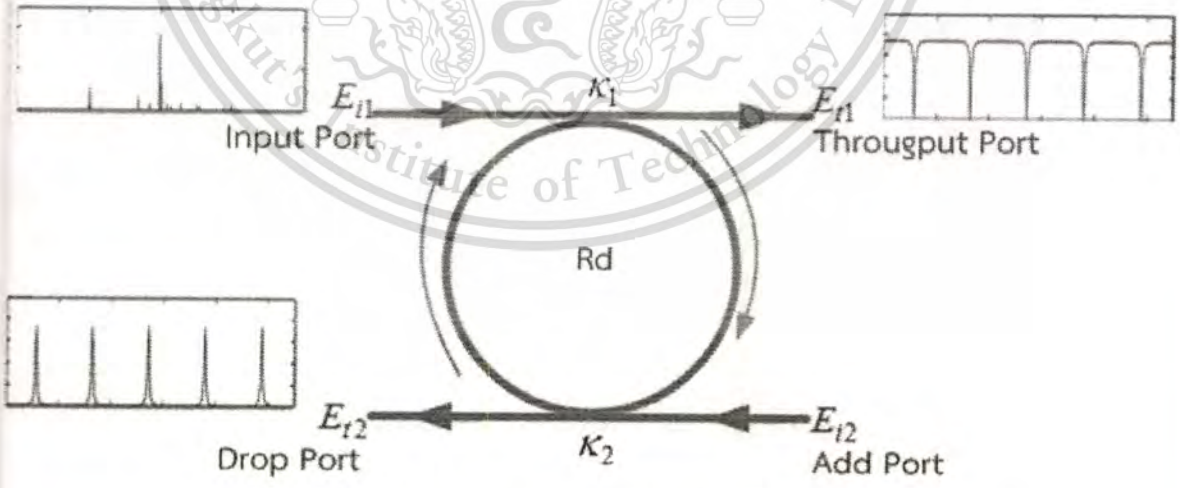

Figure 4.10 A schematic of the Add-Drop filter.

The output light of the Add/Drop filter is done corresponding to the equation (4.15) and (4.16) to send the output which is controlled and defined [53, 54] by

selecting the appropriate transmission rate of the microring resonator [55-57] and then setting the new parameters. In order to understand, it requires a constant phase $\phi = \beta L$. Chaos-off noise is handled by a particular configuration of the device parameters and the drop action with the same wavelength filter. In advance of the Add/Drop filter, we will not change the refractive index of nonlinear optical.

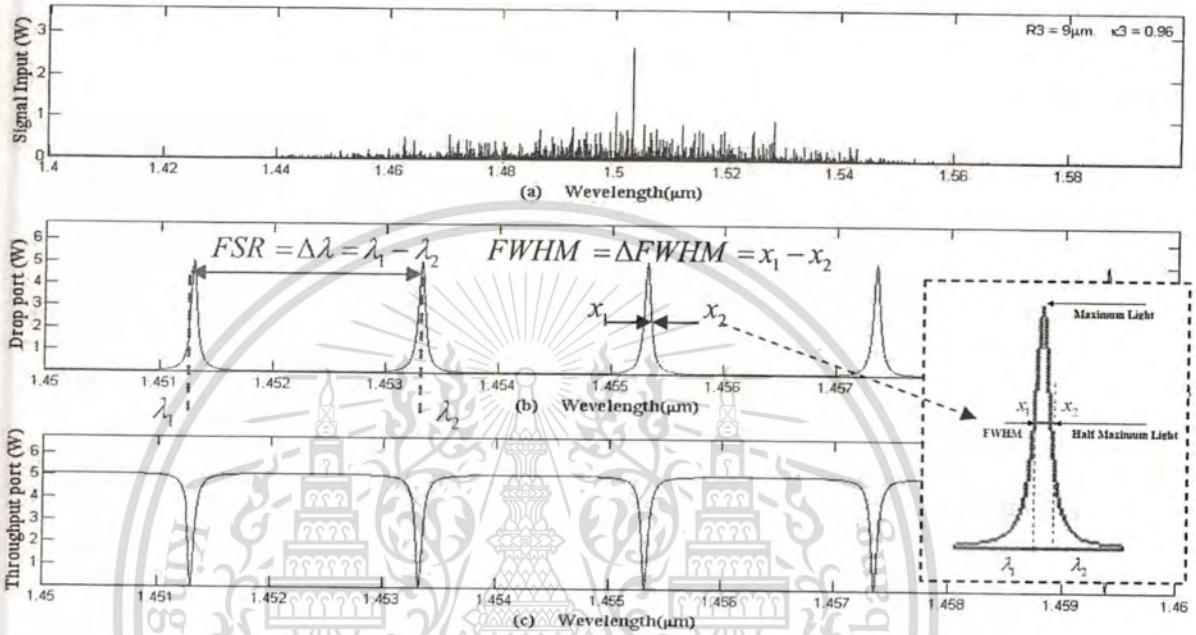

Figure 4.11 The result of Add-Drop Filter.
(a) The output of microring resonator (R_3).
(b) Drop port signal.
(c) Throughput port signal.

In figure 4.12 show a schematic of multi channel optical microring resonator system which employs to generator the large bandwidth by a Gaussian pulse propagating within the ring resonator system. The selected signals can be filtered by using the optical Add/Drop filter.

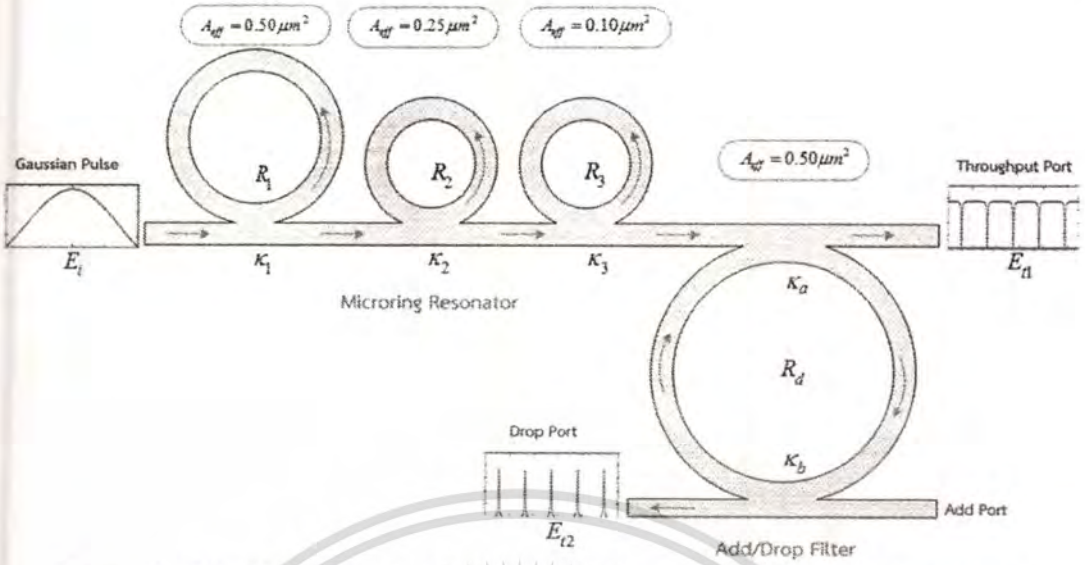

Figure 4.12 A schematic of multi channel optical microring resonator system.

4.2.1 Multi Wavelength Generation

The optical communication bandwidths (wavelength bands) is generated by Gaussian pulse propagated within a nonlinear microring resonator system. The obtained results have shown that more available wavelength bands can be achieved generation, and used in form of wavelength division multiplexing bands [58-60]. From figure 4.12 shown the Multi Wavelength Generation that the light pulse is sliced to be the discrete signal and amplified within the first ring, then signals amplification is obtained using the second and third rings. Finally, the required signals is obtained via a drop port of the Add/Drop filter by nonlinear refractive index of the microring is n_2 = 2.2 x 10^{-17} m^2/W. In figure 4.13 shown the large bandwidth signal is generated within the ring device. In applications, the specific input or output wavelength can be used generated where the suitable parameters are used and shown in the previous figures with the Gaussian pulse with center wavelength (λ_0) at 1500 nm, FWHM (δ_λ) = 0.067 nm, and peak power at 2 W. All these are input into the system as shown in figure 4.13 (a). The large bandwidth signals is produced within the first mirroring device and shown in figure 4.13 (b). The suitable ring parameters are used, e.g. ring radii R_1= 15.0 μm, R_2=R_3= 9.0 μm, and R_d= 50 μm. In order to make the system associated with the practical device [61, 62] the selected parameters of the system are fixed to n_0 = 3.34 (InGaAsP/InP), A_{eff} = 0.50 μm^2 0.25 μm^2 and 0.10 μm^2 for a microring resonator in figure 4.13, and filter signal by Add/Drop ring resonator from figures 4.14, 4.15 and 4.16 respectively, with α = 0.5 *dB/mm* and γ = 0.1. In this investigation, the coupling coefficient (kappa, κ) of the microring resonator is ranged from 0.89, 0.90, and 0.97.

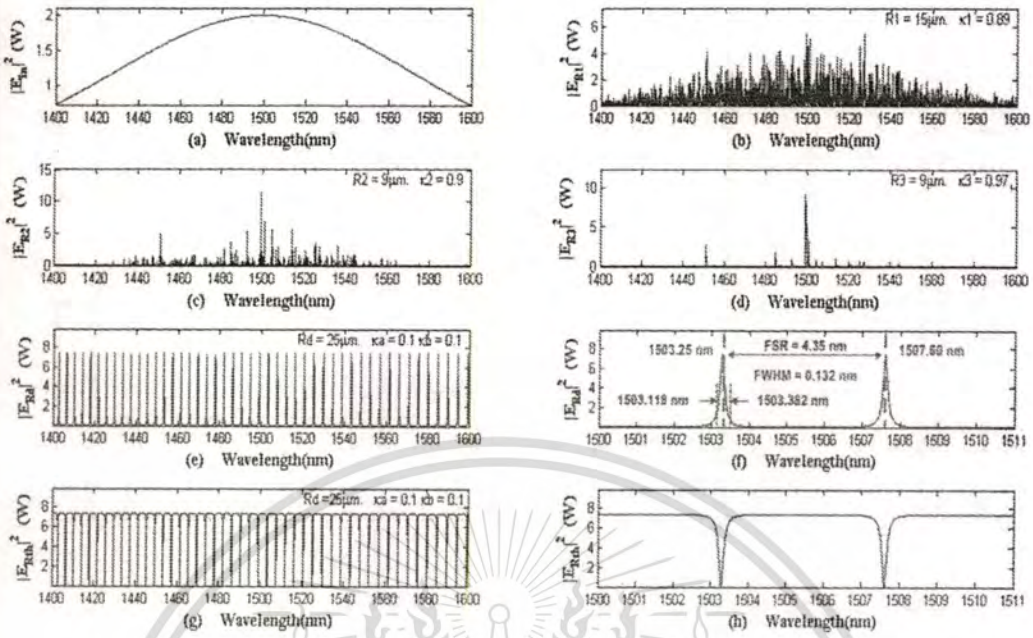

Figure 4.13 Results of the wavelength, the center wavelength at 1500 nm, with R_d =25 μm, FSR = 4.33 nm, FWHM = 0.132 nm.

The results in figure 4.13 shown the input Gaussian pulse (a), the large bandwidth signal (b), the filtering and amplifying signals (c), the storage unit (d), the drop port signal (e), the expansion of drop port signal (f), the throughput port signal (g) and the expansion of throughput port signal (h) with R_d = 25 μm, FSR = 4.33 nm and FWHM = 0.132 nm respectively. From equation (4.6), the FSR is inversely proportional to the size of the ring resonator which the ring must be small in order to achieve a high FSR. The ring radius is 25 μm, InGaAsP/InP ($n_{eff} \approx 3.3$) with FSR = 4.34 nm and from equation (4.10) the pulse width FWHM = 0.145 nm. As show above, the amount of multi wavelength band of the microring resonator is 60 channel.

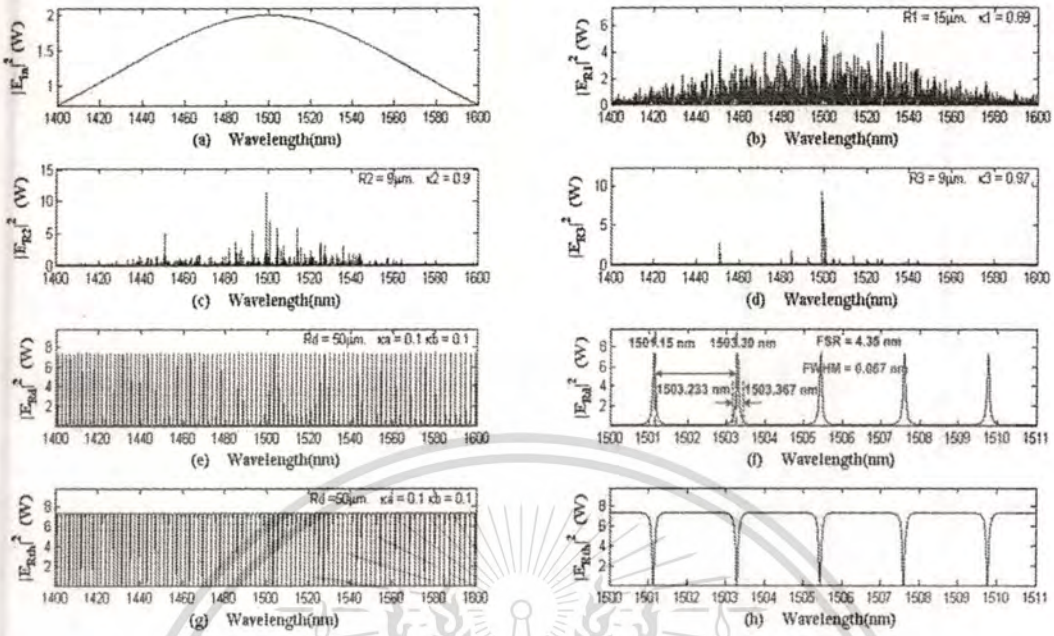

Figure 4.14 Results of the wavelength, the center wavelength at 1500 nm, with R_d =50 μm, FSR = 2.15 nm, FWHM = 0.067 nm.

The results in figure 4.14 shown the input Gaussian pulse (a), the large bandwidth signal (b), the filtering and amplifying signals (c), the storage unit (d), the drop port signal (e), the expansion of drop port signal (f), the throughput port signal (g) and the expansion of throughput port signal (h) with R_d =50 μm, FSR =2.15 nm and FWHM = 0.067 nm respectively. From equation (4.6), the FSR is inversely proportional to the size of the ring resonator which the ring must be small in order to achieve a high FSR. The ring radius is 50 μm, InGaAsP/InP ($n_{eff} \approx 3.3$) with FSR = 2.17 nm and from equation (4.10) the pulse width FWHM = 0.072 nm. As show before, the amount of multi wavelength band of the microring resonator is 100 channel.

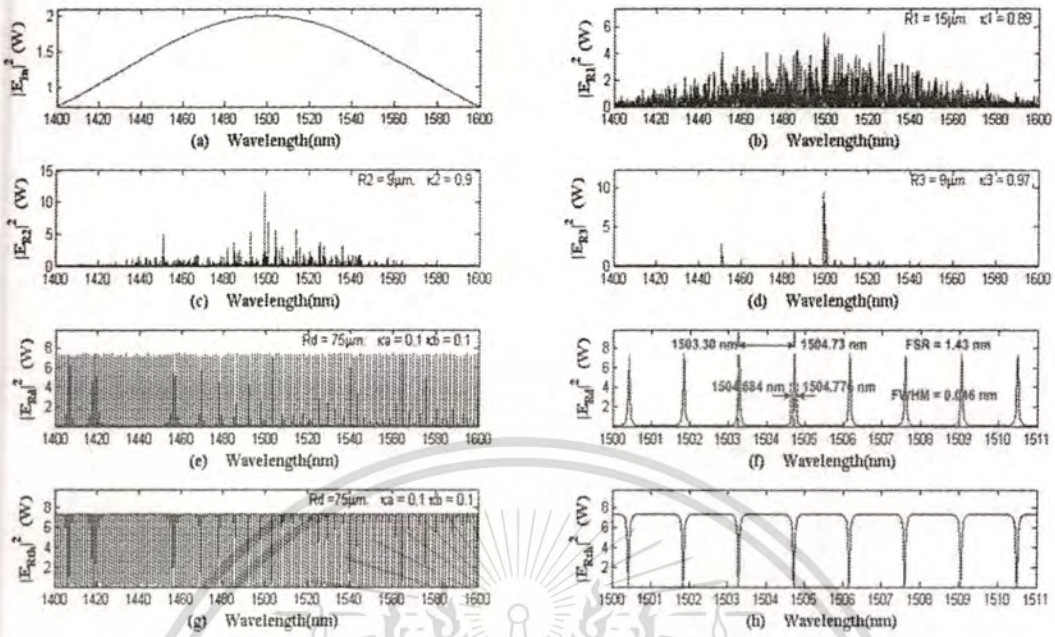

Figure 4.15 Results of the wavelength, the center wavelength at 1500 nm, with R_d =75 μm, FSR = 1.43 nm, FWHM = 0.046 nm.

The results in figure 4.15 shown the input Gaussian pulse (a), the large bandwidth signal (b), the filtering and amplifying signals (c), the storage unit (d), the drop port signal (e), the expansion of drop port signal (f), the throughput port signal (g) and the expansion of throughput port signal (h) with R_d = 75 μm, FSR = 1.43 nm and FWHM = 0.046 nm respectively. From equation (4.6), the FSR is inversely proportional to the size of the ring resonator which the ring must be small in order to achieve a high FSR. The ring radius is 75 μm, InGaAsP/InP ($n_{eff} \approx 3.3$) with FSR = 1.44 nm and from equation (4.10) the pulse width FWHM = 0.048 nm. As show result the amount of multi wavelength band of the microring resonator is 140 channel.

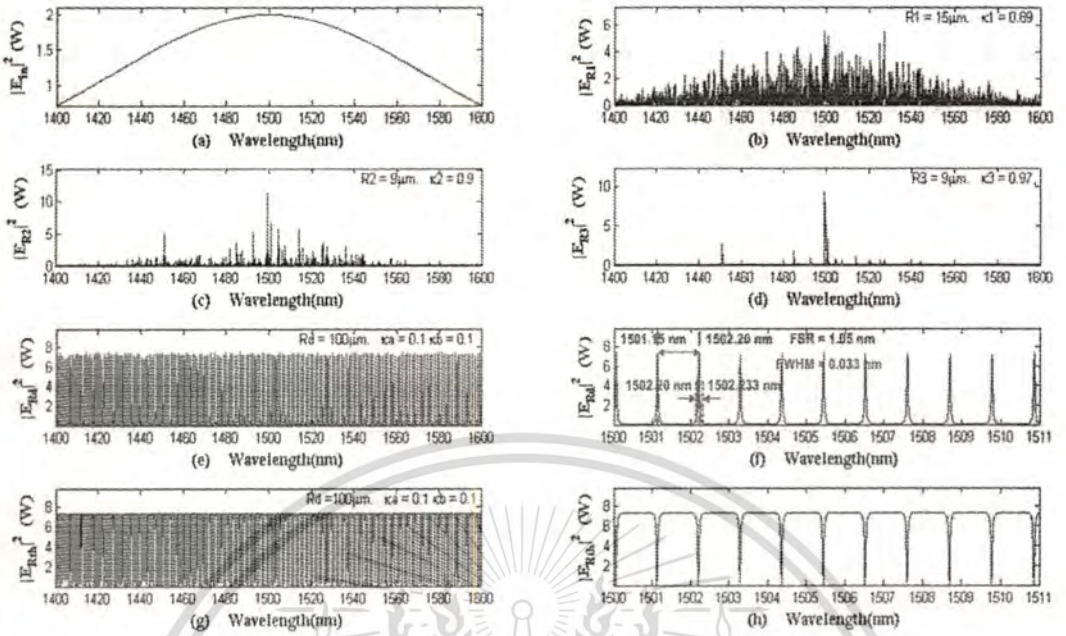

Figure 4.16 Results of the wavelength, the center wavelength at 1500 nm, with R_d =100 μm ,FSR = 1.05 nm, FWHM = 0.033 nm.

The results in figure 4.16 shown the input Gaussian pulse (a), the large bandwidth signal (b), the filtering and amplifying signals (c), the storage unit (d), the drop port signal (e), the expansion of drop port signal (f), the throughput port signal (g) and the expansion of throughput port signal (h) with R_d = 100 μm, FSR = 1.05 nm and FWHM = 0.033 nm respectively. From equation (4.6), the FSR is inversely proportional to the size of the ring resonator which the ring must be small in order to achieve a high FSR. The ring radius is 100 μm, InGaAsP/InP ($n_{eff} \approx 3.3$) with FSR = 1.15 nm and from equation (4.10) the pulse width FWHM = 0.036 nm As show in this figure the amount of multi wavelength band of the microring resonator is 180 channels.

From the simulation confirm that the generated output power with the multi wavelength band can be achieved within a small device called "microring resonator system"

4.2.2 Multi Frequency Generation

This section a design of a multi frequency generation system that uses the THz frequency generation enhancement, whereas increasing in channel capacity in term of multi frequency bands can be provided. The increasing in number of channel capacity can be obtained by increasing in frequency density, and the optical THz frequency generation and enhancement is reviewed. The advantage is that the proposed system can be implemented by using the simultaneous communication link system. We present the use of a serial ring resonator system for multi channel frequency generation [63] that can be used to form the communicate application. A system is consisted of a serial nonlinear microring resonator system for generating pulse and selecting signals that can be filtered by using the Add/Drop filter. The input pulse is a Gaussian pulse with center frequency is at 200 THz. by using the suitable simulation microring parameters. Figure 4.12 shows the multi frequency generation that light pulse is sliced to be the discrete signal and amplified within the first ring, the signals amplification can be obtained using the second and third rings. Finally, the required signals is obtained via a drop port of the Add/Drop filter, and the nonlinear refractive index of the microring is $n_2 = 2.2 \times 10^{-17}$ m^2/W. In figure 4.17, the Gaussian pulse with center frequency (f_0) at 200 THz, FWHM $(\delta_f) = 8.9$ GHz , and peak power at 2 W. The criterions above are input into the system as shown in figure 4.17 (a). The large bandwidth signals can be seen within the first microring device and shown in figure 4.17 (b). The suitable ring parameters are used, e.g. , ring radii $R_1 = 15.0\ \mu m$, $R_2 = R_3 = 9.0\ \mu m$, and $R_d = 50\ \mu m$. The selected parameters of the system are fixed to $n_0 = 3.34$, $A_{eff} = 0.50\ \mu m^2$ and $0.25\ \mu m^2$ for a microring resonator in figure 4.17, and filter signal by Add/Drop ring resonator from figures 4.18, 4.19 and 4.20 respectively, with $\alpha = 0.5$ dB/mm and $\gamma = 0.1$. In this experiment, the coupling coefficient (kappa, κ) of the microring resonator is ranged from 0.89, 0.90 and 0.97.

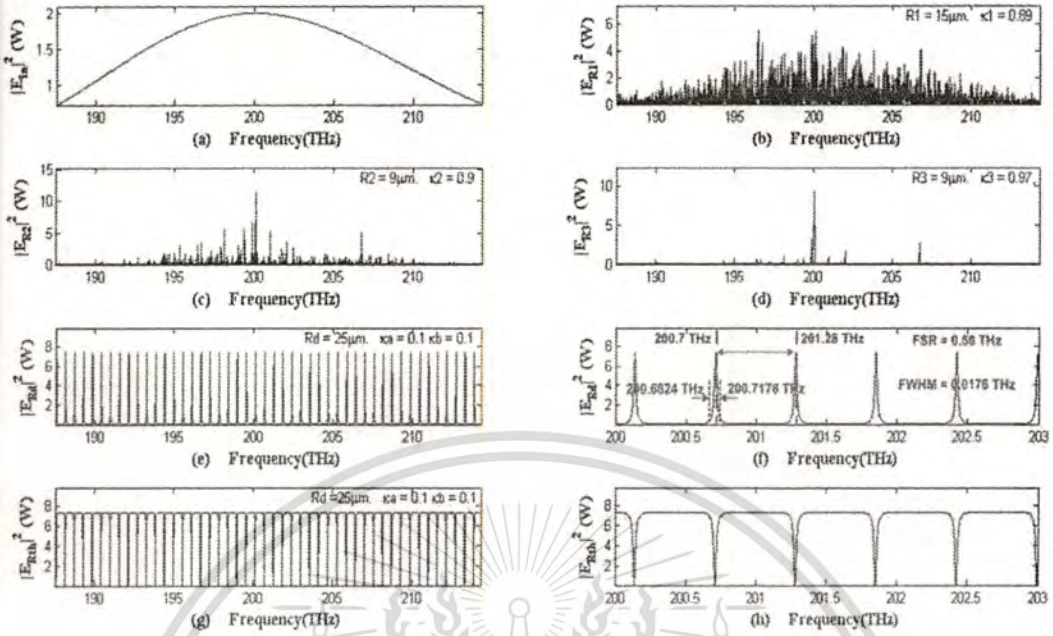

Figure 4.17 Results of the frequency, the center frequency at 200 THz, with R_d =25 μm, FSR = 571 GHz, FWHM = 17.6 GHz.

The results of figure 4.17 shown the input Gaussian pulse (a), the large bandwidth signal (b), the filtering and amplifying signals (c), the storage unit (d), the drop port signal (e), the expansion of drop port signal (f), the throughput port signal (g), and the expansion of throughput port signal (h) with R_d = 25 μm, FSR = 571 GHz, and FWHM = 17.6 GHz respectively. From equation (4.7), the FSR is inversely proportional to the size of the ring resonator which the ring must be small in order to achieve a high FSR. The ring radius is 25 μm, InGaAsP/InP ($n_{eff} \approx 3.3$) with FSR = 578.74 GHz. and from equation (4.11) the pulse width FWHM = 19.41 GHz. As show above, the amount of multi frequency band of the microring resonator is 60 channels.

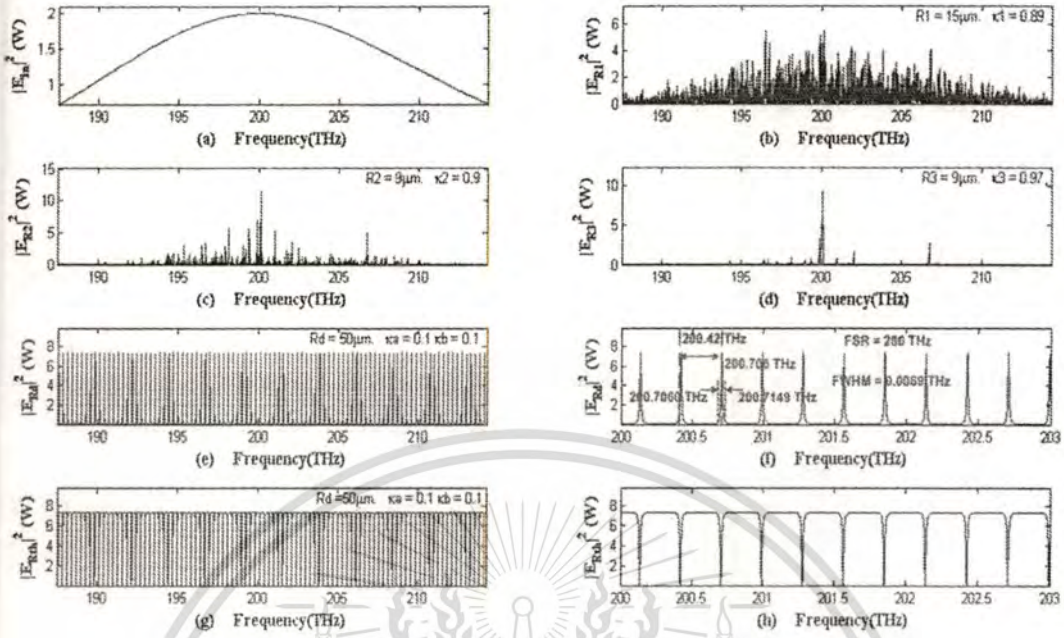

Figure 4.18 Results of the frequency, the center frequency at 200THz, with R_d =50 μm, FSR = 286 GHz, FWHM = 8.9 GHz.

The results of figure 4.18 shown the input Gaussian pulse (a), the large bandwidth signal (b), the filtering and amplifying signals (c), the storage unit (d), the drop port signal (e), the expansion of drop port signal (f), the throughput port signal (g), and the expansion of throughput port signal (h) with R_d = 50 μm, FSR = 286 GHz and FWHM = 8.9 GHz respectively. From equation (4.7), the FSR is inversely proportional to the size of the ring resonator which the ring must be small in order to achieve a high FSR. The ring radius is 50 μm, InGaAsP/InP ($n_{eff} \approx 3.3$) with FSR = 289 GHz. and from equation (4.11) the pulse width FWHM = 9.709 GHz. As show before, the amount of multi frequency band of the microring resonator is 100 channels.

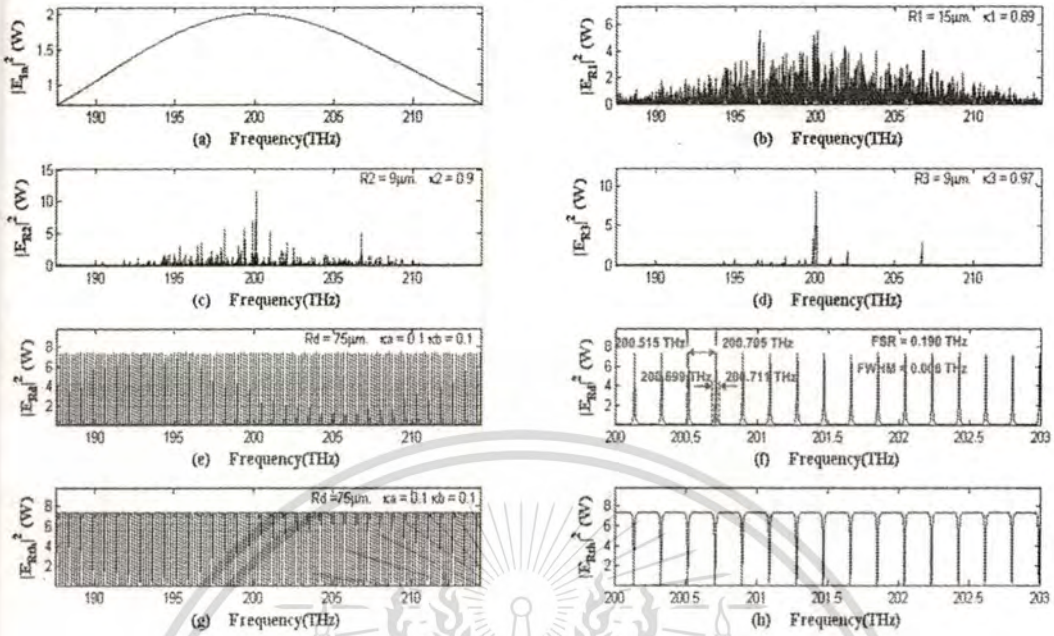

Figure 4.19 Results of the frequency, the center frequency at 200THz, with R_d =75 μm, FSR = 190 GHz, FWHM = 6 GHz.

The results of figure 4.19 shown the input Gaussian pulse (a), the large bandwidth signal (b), the filtering and amplifying signals (c), the storage unit (d), the drop port signal (e), the expansion of drop port signal (f), the throughput port signal (g), and the expansion of throughput port signal (h) with R_d = 75 μm, FSR = 190 GHz and FWHM = 6 GHz. From equation (4.7), the FSR is inversely proportional to the size of the ring resonator which the ring must be small in order to achieve a high FSR. The ring radius is 50 μm, InGaAsP/InP ($n_{eff} \approx 3.3$) with FSR = 192.91 GHz. and from equation (4.11) the pulse width FWHM 6.472 GHz. As show in this figure, the amount of multi frequency band of the microring resonator is 140 channels.

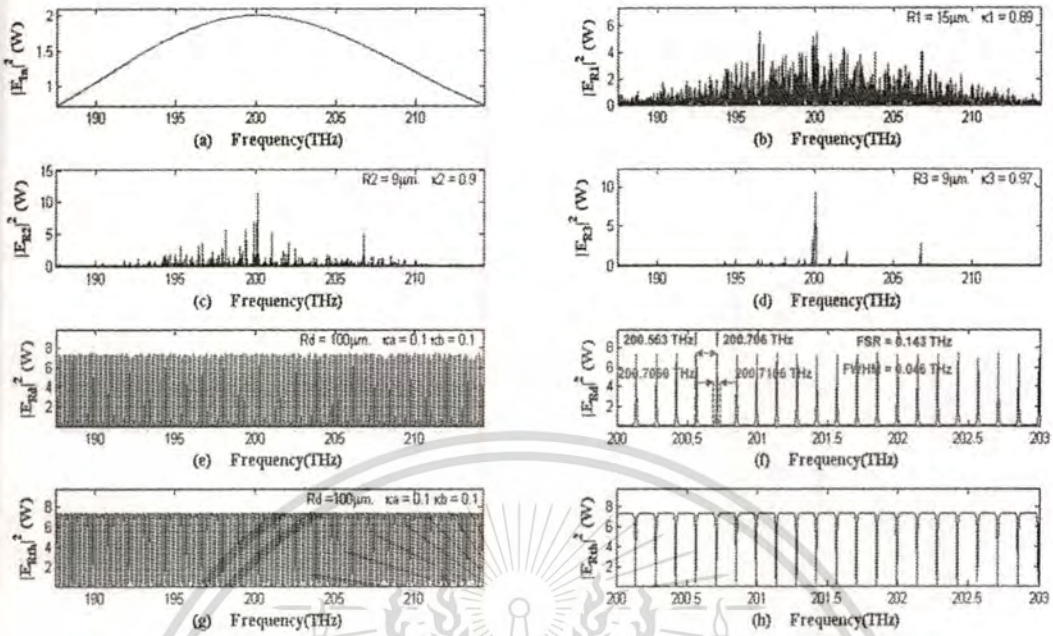

Figure 4.20 Results of the frequency, the center frequency at 200 THz, with R_d =100 μm, FSR = 143 GHz, FWHM = 4.6 GHz.

The results of figure 4.20 shown the input Gaussian pulse (a), the large bandwidth signal (b), the filtering and amplifying signals (c), the storage unit (d), the drop port signal (e), the expansion of drop port signal (f), the throughput port signal (g), and the expansion of throughput port signal (h) with R_d = 100 μm, FSR = 143 GHz and FWHM = 4.6 GHz. From equation (4.7), the FSR is inversely proportional to the size of the ring resonator which the ring must be small in order to achieve a high FSR. The ring radius is 100 μm, InGaAsP/InP ($n_{eff} \approx 3.3$) with FSR = 144.68 GHz and from equation (4.11) the pulse width FWHM = 4.854 GHz. Finally, the amount of multi frequency band of the microring resonator between 185 to 215 THz is 180 channel

By using the proposed design as shown in figure 4.12, the extended light source frequency bands is used for multi frequency generation, and the higher channel capacity can be obtained by using FSR modification and more available frequency bands, e.g., the use of system different parameters can provide more frequency bands as shown in figures 4.17, 4.18, 4.19 and 4.20. Moreover, presented system can be used with the existed optical communication applications.

Table.4.1. The used parameter of the microring resonator.

Microring resonator parameters	Value
Material type	InGaAsP/InP
Linear refractive index (n_0)	3.34
Nonlinear refractive index (n_2)	2.2×10^{-17} m^2/W
Ring radius of the microring resonator (R_1)	15 μm
Coupling coefficient R1 (κ_1)	0.89
Effective core area R1 (A_{eff})	0.50 μm^2
Ring radius of the microring resonator (R_2)	9 μm
Coupling coefficient R2 (κ_2)	0.90
Effective core area R2 (A_{eff})	0.25 μm^2
Ring radius of the microring resonator (R_3)	9 μm
Coupling coefficient R3 (κ_3)	0.97
Effective core area R3 (A_{eff})	0.10 μm^2
Ring radius of the Add/Drop Filter (R_d)	25 μm 50 μm 75 μm 100 μm
Coupling coefficient Rd ($\kappa_a = \kappa_b$)	0.1
Effective core area Rd (A_{eff})	0.50 μm^2
Coupling loss (γ)	0.1
Attenuation coefficient (α)	0.5 dB/mm

Table 4.2. The result of FSR in proposed system.

Ring Radii of Add/Drop filter (μm)	FSR			
	$\Delta\lambda_{simulation}$ (nm)	$\Delta\lambda_{calcalate}$ (nm)	$\Delta f_{simulation}$ (GHz)	$\Delta f_{Calculate}$ (GHz)
25	4.33	4.34	571	578.74
50	2.15	2.17	286	289
75	1.43	1.44	190	192.91
100	1.05	1.08	143	144.68

Table 4.3. The result of FWHM in proposed system.

Ring Radii of Add/Drop filter (μm)	FWHM			
	$\delta\lambda_{simulation}$ (nm)	$\delta\lambda_{calcalate}$ (nm)	$\delta f_{simulation}$ (GHz)	$\delta f_{Calculate}$ (GHz)
25	0.132	0.145	17.6	19.41
50	0.067	0.072	8.9	9.709
75	0.046	0.048	6.0	6.472
100	0.033	0.036	4.6	4.854

Table 4.4. The result of multi channel in system.

Ring Radii of Add/Drop filter (μm)	Multi Channel
25	60
50	100
75	140
100	180

4.4 Microring Resonator characterize evaluation using Optiwave FDTD method

The previous section explain by practical matlab simulations as computer experiments for design system with the simulation is shorter than Finite Differential Time Domain method. This section illustrate the example by the other simulation program called "Finite Differential Time Domain (FDTD)" to confirm the possibility of proposed system. Commonly, the FDTD method is a very powerful tool to performing numerical simulations and describe losses in different type of microring resonators. However, the simulation time is very long (the simulation time) and required the large amount of memory [64]. There are several researches that apply this simulation program for various applications such as microring resonators vertically coupled to bus waveguides [65] and FDTD method used to simulate microring resonator for student applications [66, 67]. Due to long computation time, this thesis will show only some experiment to confirm the plausible of our system.

(a) Design microring resonator (b) Resonant of microring waveguide

Figure 4.21 Result of whispering gallery mode of light within a mirroring resonator waveguide, InGaAsP/InP, R_1 = 15 μm, A_{eff} = 0.3 μm, n_{eff} = 3.14, n_2 = 1.3 x 10^{-13} cm^2/W, $\kappa = 0.5$, $\gamma = 0.01$, $\lambda_0 = 1550nm$.

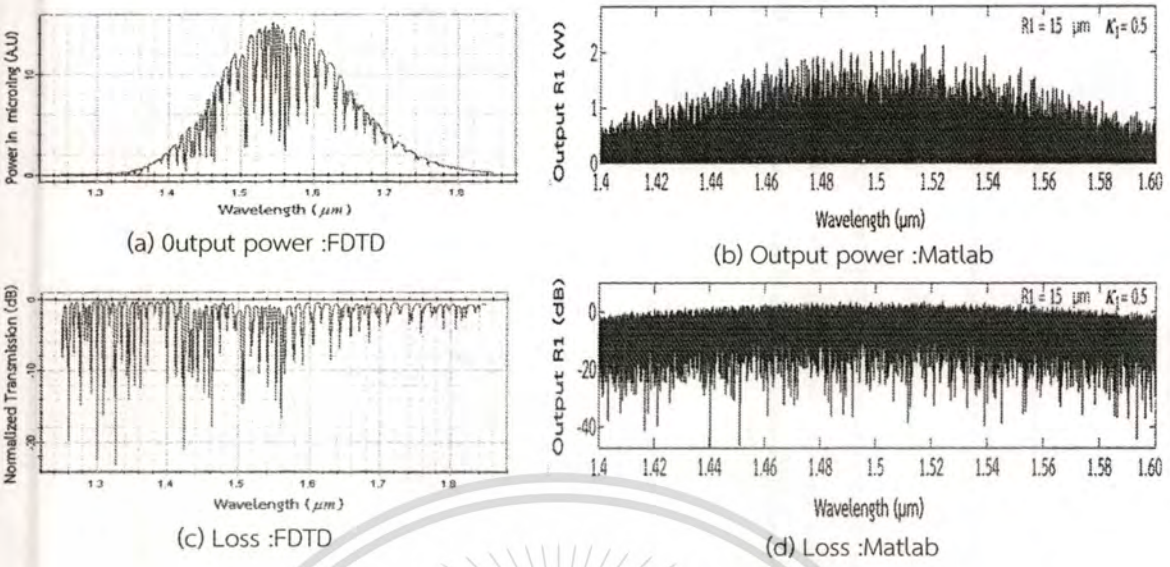

(a) 0utput power :FDTD (b) Output power :Matlab

(c) Loss :FDTD (d) Loss :Matlab

Figure 4.22 Measured transmission spectra for a 15 μm radius microring resonator TE-polarized input light is coupled into the input bus waveguide.

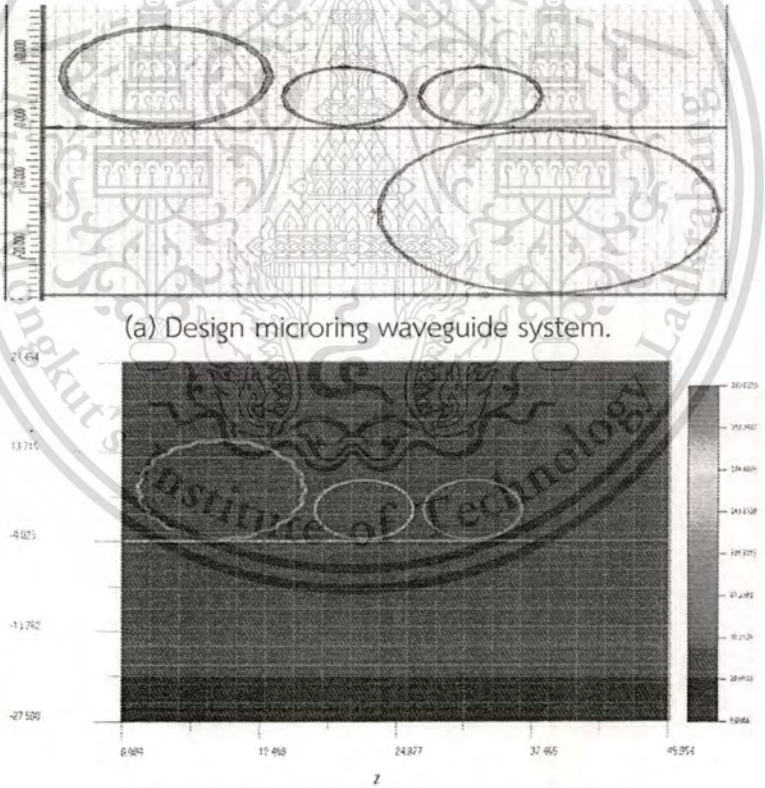

(a) Design microring waveguide system.

(b) Resonant microring waveguide system.

Figure 4.23 Result of whispering gallery mode of light within a microring resonator waveguide system (InGaAsP/InP), R_1 = 15 μm, R_2 = 9 μm, R_3= 9 μm, A_{eff} = 0.50 μm^2, 0.25 μm^2, 0.10 μm^2, n_{eff} = 3.14, n_2 = 1.3 x 10^{-13} cm^2/W, $\kappa = 0.5$, $\gamma = 0.01$, $\lambda_0 = 1550nm$.

In operation, the bandwidth signal within the microring device is generated by using a common Gaussian input which is feed into the nonlinear micro ring resonator. On the other hand the broad spectrum of light is generated after the light pulse input is propagated into the ring resonator system is shown in figure. 4.23. A system is consisted of a serial nonlinear microring resonator system that can be embedded into a small device for generating pulse and select signals.

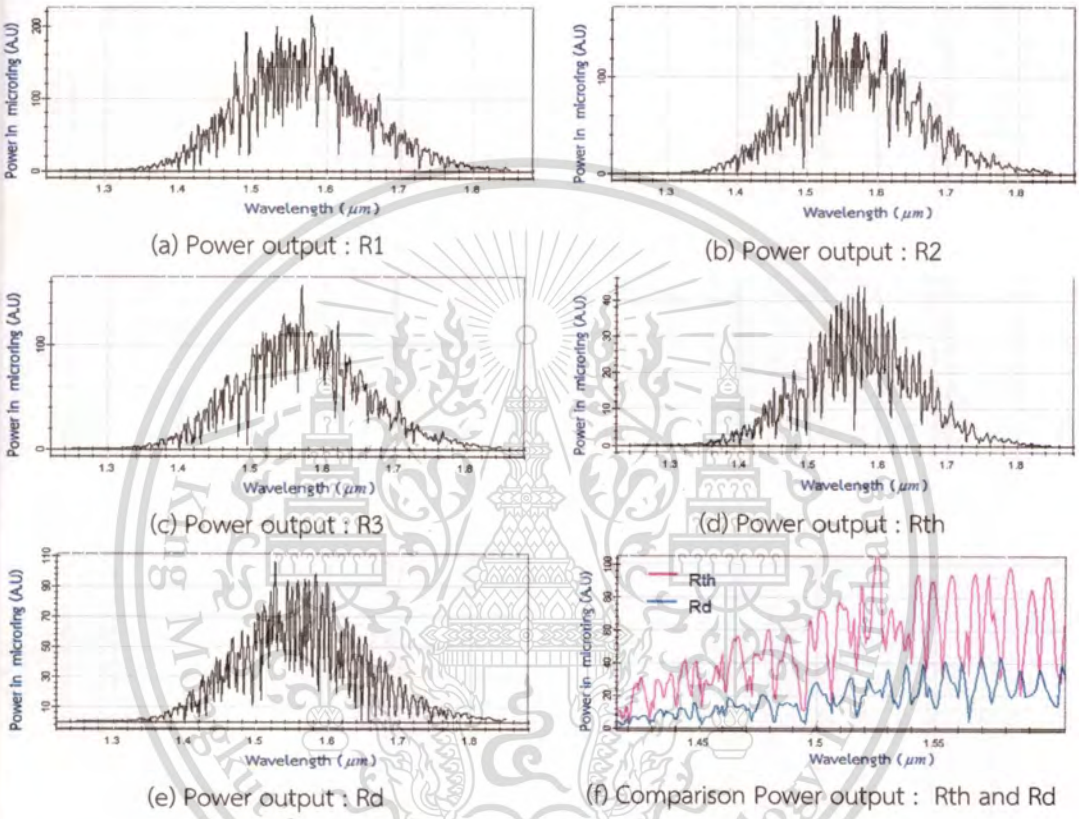

Figure 4.24 Results of the wavelength with center wavelength at 1500 nm.

The results in figure 4.24 shown the input Gaussian pulse , the output signal of first microring resonator (a), the output signal of second microring resonator (b), the output signal of third microring resonator (c). Finally, the output drop port signal (d), the output throughput port signal (e), and the comparison of throughput port and drop port signal (f) with R_d = 25 μm.

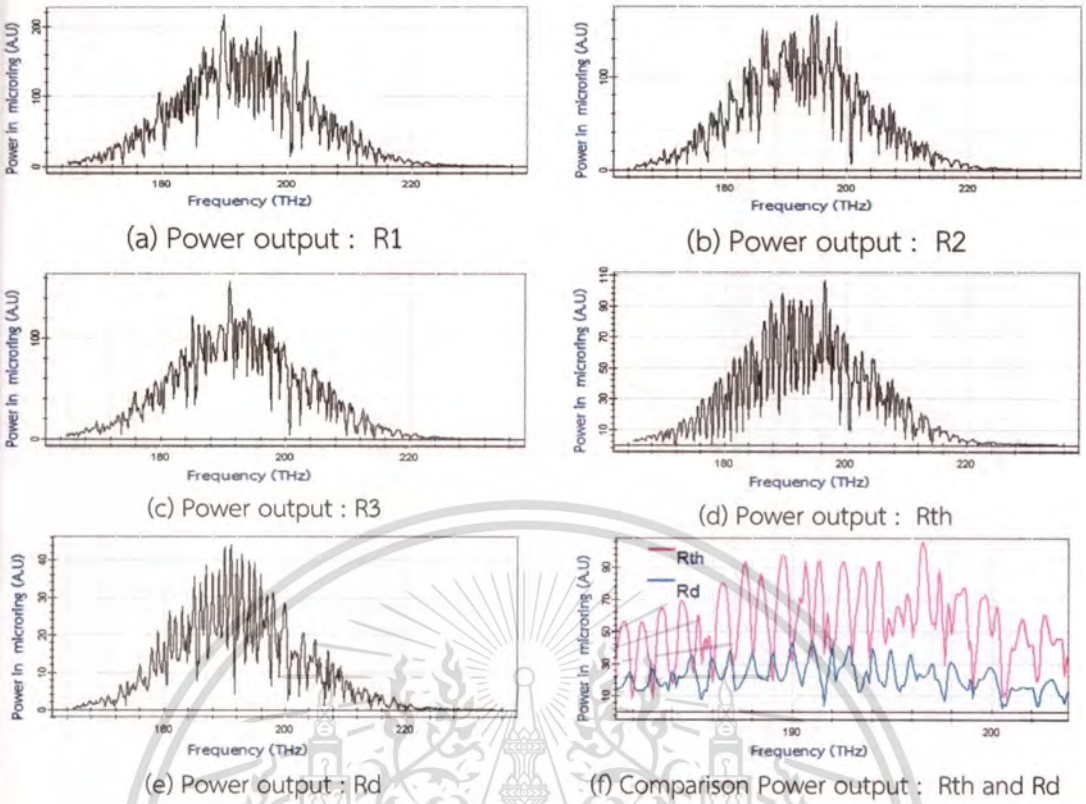

(a) Power output : R1 (b) Power output : R2

(c) Power output : R3 (d) Power output : Rth

(e) Power output : Rd (f) Comparison Power output : Rth and Rd

Figure 4.25 Result of the frequency with center frequency at 200THz.

From the FDTD results indicate that the proposed model can be fabricate and used for multi wavelength and multi frequencies generation of optical communication ranging from optical filters to lasers. These type of devices are simply integrated with other semiconductor based devices and confirm loss variation with the size and with the refractive index. In additional, the simulation were prepared for different ring radius in order to achieve these results by used the FDTD.

4.5 Results Discussion

In operation, the large bandwidth signal within the microring device is generated by using a common Gaussian pulse input which is feed into the nonlinear micro ring resonator. On the other hand the broad spectrum of light is generated after the Gaussian pulse input is propagated into the ring resonator system. The schematic of multi channel optical microring resonator is shown in figure 4.12. In order to cooperate the our system and the practical device, the selected parameters of the system are fixed to λ_o = 1550 nm, n_0 = 3.34 (InGaAsP/InP), A_{eff} = 0.50 μm^2, 0.25 μm^2 and 0.10 μm^2 for a microring resonator, α = 0.5 dB/mm, γ = 0.1. While the nonlinear refractive index is n_2 = 2.2 × 10-13 m^2/W. In this case, the wave guided loss is arraigned to be 0.5 dB/mm. The input Gaussian pulse is chopped (sliced) into the smaller signals spreading over the spectrum.

The parameter setting of the proposed system as shown the multi wavelength generation results in figures 4.13-4.16 are R_1 = 15 μm, κ_1 = 0.98, R_2 = 9 μm, κ_2 = 0.90, R_3 = 9 μm, κ_3 = 0.97 and $\kappa_a = \kappa_b$ = 0.1, respectively. For multi wavelength generation results in figures 4.13-4.16 start by the input Gaussian pulse (a), the large bandwidth signal (b), the filtering and amplifying signals (c), the storage unit (d), the drop port signal (e), the expansion of drop port signal (f), the throughput port signal (g), and the expansion of throughput port signal (h). Rd are 25 μm, 50 μm, 75 μm and 100 μm. The calculated results of FSR from equation (4.7) are 4.34 nm, 2.17 nm, 1.44 nm and 1.08 nm, while, the experimental results of FSR are 4.33 nm, 2.15 nm, 1.43 nm and 1.05 nm is indicate the same way because of the dominant nonlinear microring resonators (InGaAsP/InP) such as Kerr effect (SPM, CPM, and FWM) at the center wavelength 1500 nm by tune the different microring parameters. for originate multi wavelengths, The calculated results of FWHM from equation (4.11) are 0.145 nm, 0.072 nm, 0.048 nm and 0.036 nm while, The result simulate of FWHM are 0.132 nm, 0.067 nm, 0.046 nm and 0.033 nm is closely because of the same reason.

From the multi frequency generation results as shown in figures 4.17-4.20 which demonstrate the input Gaussian pulse (a), the large bandwidth signal (b), the filtering and amplifying signals (c), the storage unit (d), the drop port signal (e), the expansion of drop port signal (f), the throughput port signal (g), and the expansion of throughput port signal (h). R_d are 25 *μm*, 50 *μm*, 75 *μm and* 100 *μm* respectively. The calculated results of FSR from equation (4.7) are 578.74 GHz, 289 GHZ, 192.91 GHz and 144.68 GHz while, the experimental results of FSR are 571 GHz, 286 GHz, 190 GHz and 143 GHz is indicate the same way. And the calculated results of FWHM from equation (4.11) are 19.41 GHz, 9.709 GHz, 6.472 GHz and 4.854 GHz, whereas, The result simulate of FWHM are 17.6 GHz, 8.9 GHz, 6.0 GHz and 4.6 GHz is closely because of the alike above reason.

CHAPTER 5

CONCLUSIONS AND FUTURE WORK

Development of high capacity optical networks has accelerated because of emerging demands for world-wide communications. Information, interactive multimedia service, electronic commerce, and many other services are efficiently delivered online through the Internet. Optical fiber communication serves as the enable technology to realize those Internet activities. With this purpose, the generation of high frequency is essential for responsible communication demands. Therefore, we design the system which compost of a series of three microring resonators with a different radius. First ring resonator used for generation signal in chaos form by Kerr effect (nonlinear effect), the second ring resonator is used for amplification the amplitude signal and the last ring resonator is utilized for select signal (single pulse) for the output. Gaussian pulse with 200 nm pulse width, 2 W peak power, and center wavelength at 1500 nm is generated and propagated into a microring resonator system. On the way to generated the suitable output, the apposite parameters relating to the practical device such as micro ring radii, coupling coefficients, linear and nonlinear refractive indexes is preferred. Moreover, by controlling the ring resonator parameters, the appropriate output power can be obtained, and the results of good frequency FSR results (4.33 nm, 2.15 nm, 1.43 nm and 1.05 nm) have shown that they can be used to separate the two adjacent outputs. The spatial simulation output is also demonstrated that the use of the very high output frequencies (571 GHz, 286 GHz, 190 GHz and 143 GHz) within the small device is plausible. It means the nano-scale communication application can be used to the propose device, a tiny system (a chip), which will be realized in near future.

Future Work

The author is on the way to extend to study and design the other devices for generated high frequency and increased the capacity of communication system. Recently, PANDA ring resonator [68] is applied for generated THz frequency for optical network communication. For this reason, the comparison many aspect of problem between our system and other system is require. Likewise, Finite Differential Time Domain (FDTD) technique is need for confirm and evaluate our results more than Matlab 2008 only.

REFERENCES

[1] B.Mukherjee“ WDM optical communication networks progress and challenges, ” IEEE Journal of Selected Areas Commu., vol.18, no.10,10(2000) : 1810-1824.

[2] E.A.J. Marcatili, “Dielectric Rectangular Waveguides and Directional Coupler for Integrated optical,” The Bell System Technical Journal, vol. 48, (1969) : 2071-2102.

[3] E.A.J. Marcatili, “Bends in optical dielectric waveguides,” The Bell System Technical Journal, vol. 48, (1969) : 2103-2132.

[4] A. Yariv, “Critical coupling and its control in optical waveguide-ring resonator systems,”, IEEE Proton, Technol, Lett. 14, (2002) : 483-485.

[5] A. Yariv, “Universal relations for coupling of optical power between microresonators and dielectric waveguides,”, IEEE Proton, Technol, Lett. 36, (2002) : 321-322.

[6] D.G. Rabus ,“Realization of optical filters using ring resonators with integrated semiconductor optical amplifiers in GaInAsP/InP,” Der Andere Verlag, (2002).

[7] F. Michellotti, A. Driessen and M. Bertolotti, “Microresonators as building blocks for VLSI photonics”, AIP Conf. Proc. 709, Melville, New York , 2004

[8] R. Kohler,A. Tredicucci, F. Beltram, H. E. Beere, E. H. Linfield, A. G. Davies, D. A. Ritchie, R. C. Iotti and F. Rossi, “Terahertz semiconductor-heterostructure laser,” Nature, 417(2002) : 156-159.

[9] B. S. Williams, H. Callebaut, S. Kumar, Q. Hu and J. L. Reno, “3.4-THz quantum cascade laser based on longitudinal-optical-phonon scattering for depopulation,” Appl. Phys. Lett., 82(2003) : 1015-1017.

[10] T. J. Yen, W. J. Padilla, N. Fang, D. C. Vier, D. R. Smith, J. B. Pendry, D. N. Basov, and X. Zhang, “Terahertz magnetic response from artificial materials,” Science, 303(2004) : 1494-1496.

[11] B.S. Williams, S. Kumar, Q. Hu, J.L. Reno, “Operation of terahertz quantum-cascade lasers at 164 K in pulsed mode and at 117 K in continuous-wave mode,” Opt. Exp., 13(2005) : 3331-3339.

[12] W.J. Padilla, A.J. Taylor, C. Highstrete, M. Lee, R.D, Averitt, “Dynamical electric and magnetic metamaterial response at terahertz frequencies,” Phys. Rev. Lett., 96, 10(2006) : 107401.

[13] S. Mithata, N. Pornsuwancharoen and P.P. Yupapin," A Simultaneous Short Wave and millimeter Wave Generation Using a Soliton Pulse Within a nano-Waveguide, " IEEE Photon. Technol. Lett., 21(13)(2009) : 932-934.

[14] P.P. Yupapin and N. Pornsuwancharoen, "Porposed nonlinear microring resonator arrangement for stopping and storing light," Photon. Technol. Lett., 21(6)(2009) : 404-406.

[15] S. Mitatha and P.P. Yupapin, "Novel continuous spectrum generation system using a nano-waveguide for white light, short and sub-millimeter waves use", Microw. and Opt. Technol. Lett., 51(2009).(Article in press).

[16] M. Fujii, J. Leuthold and W. Freude, "Dispersion relation and loss of subwavelength confined mode of metal-dielectri-gap optical waveguides," IEEE Photon. Technol. Lett., 21(6)(2009) : 362-364.

[17] N. Pornsuwancharoen, Ali J. and Yupapin P."Optical Solitons in Nonlinear Microring Resonators: Unexpected Results and Applications," Lasers and Electro-Optics Research and Technology Series,(2009).

[18] R. Grover, P. P. Absil, V. Van, J. V. Hryniewicz, B. E. Little, O. S. King, L. C. Calhoun, F. G. Johnson, and P.-T. Ho, "Vertically coupled GaInAsP–InP microring resonators," Optics Letters, Vol. 26, (2001) : 506–508.

[19] D. Marcuse, A. R. Chraplyvy, and R. W. Tkach, "Effect of Fiber Nonlinearity on Long- Distance Transmission," Journal of Lightwave Technology, Vol. 9, (1991) : 121–127.

[20] T. A. Ibrahim, K. Ritter, V. Van, P. P. Absil, R. Grover, P. T. Ho, and J. Goldhar, "Experimental observation of optical bistability in semiconductor microring resonators," in Integrated Photonics Research (IPR), Monterey, CA, 2001.

[21] D. Anderson. "Optical filters fill many roles." WDM Solutions, 6(2001) : 97-99

[22] S. Kempainen. "Optical networking lightens carrier-backbone burden." EDN, www.ednmag.com, vol. 8, 10(1998) : 63-72

[23] E. Pawlowski et al. "Fabrication of a multichannel Wavelength-division multiplexing-passive optical net demultiplexer with arrayed-waveguide gratings and diffractive optical elements." Appl. Optics, vol. 38, no. 14, (1998) : 3039-3045

[24] Gires, F. and Tournois, P. "Interferometre utilisable pour la compression d' impulsions lumineuses modulees en frequency." C.R. Acad. Sci. Paris 258, (1964) : 6112-6115

[25] Alan Rolf Mickelson , "Physical Optics, " Van Nostrand Reinhold,(1992) : 240-254

[26] Max Born, Emil Wolf, "Principle of Optics," Pergamon Press, Oxford, fifth edition,1975

[27] G. P. Agrawal, "Nonlinear Fiber Optics," 3rd ed., Academic Press, San Diego, 2001.

[28] G. P. Agrawal," Applications of Nonlinear Fiber Optics," Academic Press, San Diego, 2001.

[29] M. F. Ferreira, "Optical solitons in fibers for communication systems," Fiber Integrat. Optics, 24, (2005) : 287-314

[30] Y. S. Kivshar and G. P. Agrawal," Optical Solitons: From Fibers to Photonic Crystals," (Academic Press, SanDiego, CA, 2003).

[31] A. Hasegawa (Ed.)," New Trends in Optical Soliton Transmission Systems," AH Dordrecht, The Netherlands, Kluwer Academic Publishers, 1998.

[32] G. P. Agrawal, "Fiber-Optic Communication Systems," 3rd ed., Wiley, New York, 2002.

[33] C. Ciminelli, V. M. N. Passaro, F. Dell'Olio, E. Armandillo and M. N. Armenise, "Three-dimesional investigation of scattering loss in InGaAsP-InP and Silica-on-Silicon bent waveguides," J. of European Optical Society, 2008

[34] R. W. Boyd. "Nonlinear Optics." 2nd ed. Academic Press, Inc., 2003

[35] T.A. Ibrahim. "Nonlinear Optical Semiconductor Micro-Ring Resonators," Ph. D. Thesis of University of Maryland. 2003.

[36] P.P. Yupapin, Chart Teeka and P. Chitsakul, "Mathematical Simulation of Nonlinear Effects in Microring Resonator," IEEECET-06, NanoSingapore, (2006): 316-321.

[37] D. A. B. Miller, S. D. Smith, and A. Johnston. "Optical bistability and signal amplification in a semiconductor crystal: Applications of new low-power nonlinear effects in InSb." Appl. Phys Lett., vol. 35, no. 12, (1979) : 658–660

[38] P. Mandel, S. Smith, and B. Wherrett. "From Optical Bistability Towards Optical Computing." North-Holland, 1987

[39] H. M. Gibbs. "Controlling Light with Light." Academic Press Inc., 1985

[40] K. Otsuka. "Pitchfork bifurcation and all-optical digital signal processing with a coupled-element bistable system." Opt. Lett., vol. 14, no. 1,(1989) : 72-74

[41] L. M. Zhao, D. Y. Tang, F. Lin and B. Zhao. "Observation of period-doubling bifurcations in a femtosecond fiber soliton laser with dispersion management cavity." Opt. Exp. vol. 12, no. 19, (2004) : 4573-4578

[42] Fan Yi Lin and Meng Chiao Tsai. "Chaotic communication in radio over fiber transmission based on optoelectronic feedback semiconductor laser." Opt Exp., vol. 15, no. 2, 1 (2007) : 302-311

[43] K.Ikeda, H. Daido and O. Akimoto. "Optical turbulence: Chaotic behavior of transmitted light from a ring cavity." Phys. Rev. Lett., vol. 45, (1980) : 709-712

[44] J. Ohtsubo, "Chaos Synchronization and Chaotic Signal Masking in Semiconductor Lasers With Optical Feedback," IEEE J. of Quantum Electronics, Vol. 38, No. 9, (2002) : 1141-1154.

[45] C. Juang,T.M. Hwang, J.Juang,and Wen-wei Lin. "A Synchronization Scheme using self-pulsating laser diode in optical chaotic communication ". IEEE J. Quantum Electron., Vol. 36, (2000) : 300-304.

[46] D. Deng and Q. Guo, "Ince-Gaussian Solitons in Strongly Nonlocal Nonlinear Media,"Opt. Lett., 32(2007) : 3206-3208.

[47] Q. Xu and M. Lipson, "All-optical Logic based on Silicon Microring Resonators," Opt. Exp. 15(3)(2007) : 924-929.

[48] P.P. Yupapin and W. Suwancharoen, "Chaotic Signal Generation and Cancellation using a Microring Resonator Incorporating an Optical Add/Drop Multiplexer," Opt. Commun., 280(2)(2007) : 343-350.

[49] P. Saeung and P.P. Yupapin, "A Design of Optical Ring Resonator Filters for WDM Applications", JNOPM, Special Issue Volume, November, 2008.

[50] Apollo Photonics. Apss Apollo Application Note on Microring Resonator, Computer-Aided Design and Simulation APN-APSS-Ring Resonator

[51] W. Suwancharoen, S. Thongmee and S. Chaiyasoonthorn and P.P. Yupapin, "Chaotic Signal Filtering Device using a Serial Connection of Micro-Ring Resonators," JNOPM, Special Issue Volume, 11(2008).

[52] Dominik G. Rabus, "Realization of Optical Filters using Ring Resonators with integrated Semiconductor Optical Amplifiers in GaInASP/InP." Ph.D. Thesis of University of Berlin. 2002.

[53] P. Saeung, W. Kunnam, P.P. Yupapin and W. Techitdheera, "Mathematical Simulation of Fiber Optic Ring Resonator for Optical Add/Drop Multiplexing," SPIE Vol. 6038, (2005) : 6038 1A-6038 5A

[54] W. Siririt, S. Mitatha, O. Pingern, and P.P. Yupapin," A novel temporal dark-bright solitons conversion system via an add/drop filter for signal security use," Optik - International Journal for Light and Electron Optics, 2009.

[55] P.P. Yupapin, P. Saeung and C. Li, "Characteristics of complementary ring-resonator add/drop filters modeling by using graphical approach," Opt. Commun., 272(2007) : 81-86.

[56] S. Mitatha, K. Dejhan, S. Chaiyasoonthorn and P.P. Yupapin," Atto Second Pulse and Its Beyond Generation Based on Muti-stage Microring Resonators," Advanced Materials Research, Vol. 55-57, (2008) : 485-488.

[57] P.P. Yupapin, P. Yabosdee and P. Phiphithirankarn, "Entangled photon generation in a nonlinear microring resonator for birefringence based sensing application," International Journal of Light and Electron Optics, 2008.

[58] Q. Li, Z. Zhang, F. Liu, M. Qiu, and Y. Su, "Dense wavelength conversion and multicasting in a resonance-split silicon microring, "Applied Physics Lett 93, 081113 (2008)

[59] D. Syvridis, H. Simos, S. Mikroulis ,and A. Kapsalis," Microring based devices for telecommunication applications," Proc. of SPIE Vol. 7211 (2009) : 1-15

[60] B. E. Little, S. T. Chu, H. A. Haus, J. Foresi, and J.-P. Laine," Microring Resonator Channel Dropping Filters," JOURNAL OF LIGHTWAVE TECHNOLOGY, VOL. 15, NO. 6, 6 (1997) : 998-1005.

[61] Y. Kokubun, Y. Hatakeyama, M. Ogata, S. Suzuki, and N. Zaizen, "Fabrication Technologies for Vertically Coupled Microring Resonator with Multilevel Crossing Busline and Ultracompact-ring Radius," IEEE J. Sel. Top. Quantum Electron., 11(2005) : 4–10.

[62] Y. Su, F. Liu, and Q. Li, "System Performance of Slow-light Buffering and Storage in Silicon Nano-waveguide," Proc. SPIE 6783, (2007)67832P.

[63] M. A. Popović, C. Manolatou and M. R. Watts, "Coupling-induced resonance frequency shifts in coupled dielectric multi-cavity filters," OPTICS EXPRESS,Vol. 14, No. 3.,6 (2) (2006) : 1208-1222.

[64] A. Fazacas, P. Sterian, " Finite-Difference Time-Domain Method (FDTD) used to simulate Micro-ring resonator for student applications," Journal of Optoelectronics and Advanced Materials, Vol. 14, No. 3-4, (3-4)(2012):344 - 349.

[65] S. J. Choi, K. Djordjev, P. D. Dapkus, W. Lin, G. Griffel, R. Menna, and J. Connolly "Microring Resonators Vertically Coupled to Buried Heterostructure Bus Waveguides," IEEE Photonics Technology Letters, VOL. 16, NO. 3, (3)(2004):822-830.

[66] J. H. Song, H. S. Lee, O. B. Hoan, S. G. Lee, S. G. Park and E. H. Lee , " Design of Nanoring Resonators Made of Metal-insulator-metal Nanostrip Waveguides," Journal of the Korean Physical Society, Vol. 57, No. 6, (12)(2010):1789-1793.

[67] V. M. N. Passaro , F. Dell'Olio and F. D. Leonardis , "Ammonia Optical Sensing by Microring Resonators," *Sensors,* (7)(2007): 2741-2749.

[68] Preecha P. Yupapin and Soomboon Nimcome, "Conjugate mirror by a panda ring circuit," Science Innovation, Vol. 1, No. 1, (2)(2013):1-4.

APPENDIX

LIST OF PUBLICATIONS

1. P. Udomariyasap, S. Noppanakeepong, S. Mitatha and P.P. Yupapin, "THz Light Pulse Genneration and Storage within an Embedded Optical Waveguide System," IEEE International NanoElectronics Conference,IEEE INEC ,Hong Kong, China, 2010.
2. P. Udomariyasap, S. Noppanakeepong, S. Mitatha and P.P. Yupapin, "Novel Molecular Networking via a Simultaneous Optical Wireless Up-down Link Systems," Progress In Electromagnetics Research Symposium, PIERS, Xi'an, China, 2010.
3. P. Udomariyasap, S. Noppanakeepong, S. Mitatha and P.P. Yupapin, "THz Light Pulse Generated and Storage by using a Gaussian Pulse within a Waveguide System,", International Journal for Light and Electron Optics , Optik,2011. Journal (Impact Factor:2010:0.454) (Article in press)
4. P. Udomariyasap, S. Noppanakeepong, S. Mitatha and P.P. Yupapin, "Novel Multi Channel RFID using THz Frequency Enhancement," Japan Society for Simulation Technology Conference, JSST , Tokyo, Japan, 2011.
5. S. Mitatha ,P. Udomariyasap, S. Noppanakeepong, and P.P. Yupapin, "Highly Capacity RFID Generated by a Soliton Pulse within a PANDA Ring Resonator," Microwave and Optical Technology Letters, MOP, 2011. (Impact Factor: 2010:0.685)

BIOGRAPHY

Name: Mr.Pongputhai Udomariyasap
Date of Birth: September 25th, 1979.
Born: Mukdahan, Thailand.
Current Address: 15, Soi. Sriworabut, Mukdahan-Dontan Rd., Sub-District. SI BUN RUEANG, Muang Mukdahan, Mukdahan, Thailand, 49000.
E-mail: pongputhai@hotmail.com

Education

- Bachelors of Engineering in Electrical and Telecommunication Engineering, Faculty of Engineering, Rajamangala Institute of Technology, Pathum Thani, in 2004.
- Master of Engineering in Telecommuniations Engineering, Faculty of Engineering, King Mongkut's Institute of Technology Ladkrabang, Bangkok, in 2008.

Scholarship

Telecommunications Research and Industrial Develop Institute(TRIDI), National Telecommunications Commission (NTC) Fund (Grant No. PHD / 002 / 2552) to Mr. Pongputhai Udomariyasap and Assistant Professor Dr.Suthichai Noppanakeepong is acknowledged.